Optical Intersatellite Link

A Study for Global Satellite Communications Networks

by Claude Bélisle and Caroline Delisle

CRC TN NO. CRC-98-004

TAWA, July 1998

Communications
Research Centre
Centre de recherches
sur les communications

ABSTRACT

Recently, there has been renewed interest in intersatellite link (ISL) communications, driven mainly from international projects on large-scale satellite-communications systems such as Iridium and Teledesic. In some of these projects, tens of satellites will be orbiting the earth to provide worldwide communications. To provide high bandwidth communications links at the lowest possible cost, intersatellite links are being developed for a number of the proposed systems. Because of the bandwidth and mass and volume requirements, optics has been chosen as the best technology to implement ISL.

In this report, a technical assessment of Optical Intersatellite Link (OISL) is done. Various parameters, such as link range, pointing azimuth and elevation are computed to define specifications for telescope gimbals and aperture size as well as optical power. These parameters could later serve to identify critical sub-systems of present technology and focus the research activities towards new avenues. In the first part of the report, the characteristics of the most promising satellite constellations are reviewed with respect to intersatellite links. Then orbital analysis are made on Teledesic and Celestri constellations to derive telescope critical parameters such as scanning angles and slew rates. The report continues with a link budget analysis to derive the communication package requirements such as optical power, telescope size, noise level, bit-error rates.

The activities surrounding this report were undertaken under the sponsorship of the Canadian Space Agency.

EXECUTIVE SUMMARY

The demand for commercial satellite communications services is expanding at a rate never seen before. Hundreds of satellites are being planned for deployment within the next decade to provide a wide variety of communications services such as internet, video-conferencing, fix and mobile communications over the entire globe. In order to minimize the up and down link traffic that such world-wide-coverage constellations would require, and to minimize the number of terrestrial gateways, intersatellite links are being developed for a number of the proposed systems. Because of tight mass, size and power requirements, optics has been selected as the preferred technology to provide the link.

In this report, a technical assessment of Optical Intersatellite Link (OISL) is done. Various parameters, such as link range, pointing azimuth and elevation are computed to define specifications for telescope gimbals and aperture size as well as optical power.

In a first section, the orbital and ISL requirements for systems which are most likely to be deployed are given. Those include, Astrolink, Iridium, Spaceway, Orblink, Celestri and Teledesic. Then two systems, Teledesic, with 288 satellites in a polar orbit and Celestri with 63 satellites in a 48° inclined orbit are analyzed in greater details. Orbital simulations are done to evaluate the cross-link parameters such as range, azimuth, elevation as well as the variation rates. It is found that the requirements for the Teledesic system are more stringent than for Celestri. For Teledesic, the AER values are ±110°, ±15° and 4300km, whereas those numbers change to ±75°, ±6° and 6000km for Celestri. The rate of change for the AER values also greatly differs and that is due to the fact that the orbital inclination of Teledesic creates a seam across which satellites are moving in opposite directions. This forces the telescope to swing at a rate of 15°/min for azimuth and 2°/min in elevation. However, the most stringent requirement for the Teledesic optical terminals is the movement of the telescope for reacquisition. Because of the polar orbits, communications links are broken near the poles and are to be re-established on the other side with a different satellite. This forces the telescope to be repositioned during the silent period. A slew rate of 6°/sec is required by the system designers.

In a second section, link budgets are computed and bit-error-rates (BER) are given for amplitude shift keying modulation, the modulation of choice for those systems. It is found that for a 10 cm telescope aperture, a transmit optical power of 1W is required to obtain an uncoded BER of 10^{-6}, at 2.5 Gbps on 5000 km link.

TABLE OF CONTENTS

TABLE OF FIGURES

1 INTRODUCTION

1.1 Scope

This report covers the technical assessment of Optical Intersatellite Link (OISL) as per the Canadian Space Agency / Communications Research Centre R&D agreement of 6 June 1997.

1.2 General

The demand for commercial satellite communications services is expanding at a rate never seen before. Hundreds of satellites are being planned for deployment within the next decade to provide a wide variety of communications services such as internet, video-conferencing, fix and mobile communications over the entire globe. For many years there has been a number of satellite systems providing telephone communications links and broadcast services such as television. Mobile satellite services, such as MSAT and INMARSAT are currently providing low bandwidth (voice and fax) communications to ships, aircraft and mobile terrestrial terminals. All of the systems so far have been based on analog RF transponders, allowing "bent pipe" communications between ground stations, and most of the satellites were located at geosynchronous (GEO) locations. With the IRIDIUM project, a new type of satellite system has emerged. IRIDIUM was the first to file for multiple low earth orbit satellites linked with intersatellite links (ISL) to provide on-orbit switching of digital signals, moving the telephonic switching and long-haul communications from terrestrial networks to orbit. Following this, a number of other systems have been proposed, as shown in Tables 1 and 2. These tables show satellite systems in the Ka-band only. A number of other systems have also been filed at other frequency bands.

Table 1 FCC filings for fixed satellite services in the 28 GHz Ka-band [1]

Sponsoring Organization (Owner)	Satellite Program Name	Proposed services (see Table 2)
AT&T	VoiceSpan	1,2,7,G
Comm Inc. (Motorola)	Millenium	2,3,4,6,G
EchoStar	EchoStar	4,6,IR
GE Americom	GE Star	2,4,6,G
Hughes	Spaceway/Galaxy	5,8,G
Lockheed Martin	AstroLink	2,4,6,G
Loral	CyberStar	8,G
Teledesic	Teledesic	2,3,4,6,7,8,G

Table 2 Legend to Table 1 proposed services [1]

Proposed Services Code	Proposed Communications Services
1	Messaging
2	Voice Communications (Telephony)
3	Facsimile Services
4	Video services, including video conferencing
5	Direct-to-home or other broadcast video
6	High speed switched data or computer data
7	Software distribution
8	Multimedia or two-way interactive services
G	Global or intercontinental service
IR	Interregional or Transcontinental

Most of the new satellite communications systems filed are to provide global or transcontinental services. Obviously, a single satellite can not provide such services. Therefore, communications links between satellites must be established. Relying on terrestrial gateways to provide such links may not be economically acceptable since scare uplink/downlink capacity would be used simply to provide long-haul communications. Moreover, those gateways must be maintained and some of them will need to be located in unfriendly territories. Intersatellite links (ISL) can alleviate such a problem by providing a direct link between satellites.

Numerous studies have been conducted in the past on the feasibility of ISL using both RF and optical technologies. A number of ISLs have been experimented to date but mainly using microwave frequencies in various bands such as 23 GHz, 38 GHz and 60 GHz. However, as the communications bandwidth increases, the requirement for higher gain links forces the use of optical technology. Not only can optics support higher data rate links but it can do it with smaller, cheaper and lighter systems. The high-bandwidth constellation satellites programs (Teledesic, Celestri) have elected optics as their number one choice for intersatellite links.

In Canada, research on optical intersatellite links began in the early 1980 under the military recoverable program managed by the Communications Research Centre (CRC). Various studies on components and system architectures were done [2-4] and two laboratory prototypes were built [5-7] In 1990, the Canadian Space Agency (CSA) funded a study [8] to define the status of the optical technology and to design a complete optical system which would respond to some very specific communication requirements.

In 1996, the CSA, through the Advanced Satcom program, awarded two contracts to the industry for system study on intersatellite links. One study evaluated the optical technology [9] while the other one investigated an RF implementation [10]. In 1997, two new contracts were issued to industry for the development of hardware capability for optical ISL [11-12]. CAL Corporation is to develop a telescope steering mechanism that will permit pointing and tracking. COMDEV is to develop the overall optical front end including the lasers and detectors. Those

two contracts are to address short-term requirements dictated by the industry for the deployment of their satellite services.

1.3 Objective and Scope

The objective of the work introduced in this report is to develop a basic understanding of the current ISL requirements and related optical technologies in order to initiate technology development for the next generation of optical ISL systems.

To accomplish this, ISL system requirements will be analyzed for the planned satellite communications systems. The analysis will cover both pointing and tracking as well as the communications parameters. It is not the intention of this report to provide solutions for future systems but rather to develop in-house expertise with the present systems in order to identify potential shortcomings or possible improvement areas.

1.4 Report Organisation

The report is divided into four sections with this introduction being Section 1. In section 2, the parameters of interest to ISL for the satellite services that have elected intersatellite links at time of their filing to the FCC are given. In section 3, an orbital analysis is done on a few systems to obtain information about the pointing and tracking requirements. In section 4, the communications link is analyzed in terms of bit error rate, signal-to-noise ratio, optical power, and telescope diameters.

2 SYSTEM DESCRIPTION

In this chapter, the parameters of interest to ISL are given for a number of satellite services that have elected ISL as a way of relaying their information from of satellite to satellite. This information will be used for defining the system requirements and component specifications. The basic intersatellite links requirements for each of those systems are summarized in Table 3 where orbital, constellation and crosslink parameters are listed. It must be noted that the parameters listed may still be changing as the system definition evolves. This is particularly the case for the Teledesic system.

Most of the systems filed before the FCC have specified microwave frequency for the ISLs. Most certainly, this was to insure microwave spectrum allocation, since the RF spectrum is very limited and has severe contingency, which is not the case for the optical band. Filing a request for an RF link bears no obligation to use it, and an optical link could be employed instead.

	AstroLink [1]	Iridium [3]	SpaceWay [4]	OrbLink	Celestri	Teledesic
Type	GEO	LEO	GEO	MEO	Hybrid LEO/GEO	Global LEO
Eccentricity	0	Circular polar	0	0	0.0013	Circular
Altitude	35786 km	780 km	35786 km	9000 km	1400 km	1350 km
Inclination	0	86.4 degrees	0	0	48 degrees	90 degrees
Location	38E / 115E / 172.5E / 21.5W / 97W	N/A	25E / 111E / 175E/ 49W / 99W / 101W		N/A	
No of planes	5	6	6		7	12
Plane spacing	uneven		Uneven		51.43 degrees	
Plane phasing	N/A		N/A		28.57 degrees	Random
No of satellites / plane	2/ 2/ 1/ 2/ 2	11	9 total initially, 17 final total	1	9	24
ISL Links per payload	2	4.		2	6.	8.
Frequency	54.25 - 58.2GHz 59.0 - 64.0 GHz	23.18 - 23.38 GHz	Optical	Optical	Optical	59.5 – 60.5GHz or 62.5 63.5GHz
Data rates	1 Gbps	25 Mbps		7 Gbps	7.5 Gbps	2.5 Gbps

Table 3 Major satellite system parameters

3 ORBITAL ANALYSIS

In this chapter, the orbital parameters of importance for the design of intersatellite links will be defined. Range, azimuth and elevation angles, as well as their rate of change will be computed. This information will be of use for the definition of a set of specifications for the pointing and tracking, and for the communications system, (optical power, telescope size).

In the first section, the simulation tools and parameters will be described. In sections 2 and 3, the Teledesic and Celestri systems will be studied based on the parameters given in Table 3. In section 4, the frequency variation, or Doppler shift, resulting from the approach or separation of two satellites will be analyzed. Note that the simulation techniques described in this chapter could easily be applied to any other systems.

3.1 Orbital Analysis Software Description

The orbital analysis has been done using Satellite Tool Kit (STK 4.0) software produced by Analytical Graphics Inc. A Keplerian, J2 and J4 orbital propagators were available for simulation. The Keplerian motion propagator considers the Earth to be a point mass with no perturbations. J2 Perturbation (first-order) and J4 Perturbation (second-order) propagators account for secular variations in the orbit elements due to Earth oblateness. None of those three propagators model atmospheric drag or solar and lunar gravitational forces. For the analysis done in this report, it was found that the J2 and J4 models gave similar results, to within one percent, as a Keplerian propagator. The Keplerian propagator was then used for simplicity. Classical coordinates, based on altitude, orbit inclination and mean anomaly was used. Table 4 gives a description of the orbital parameters used in the simulation. Figure 1 shows pictorially some of the parameters listed in Table 4.

Table 4 Description of the orbital parameters used in the simulation.

Start / Stop time:	Corresponds to the start and stop time of the orbit simulation. The start time was set arbitrarily to 1 January 1997 at 00:00:00hrs for all simulations. The stop time was set to simulate a complete orbit.
Orbit epoch:	Sets the time at which the established orbital parameters are valid. The simulation start time was used in the analysis.
Orbit inclination	Those values are specific to each system and are given in Table 3.
Apogee / Perigee Altitude:	The apogee and perigee altitudes are the distances between the surface of the Earth and the point of maximum and minimum radius on the elliptical orbit respectively. These values are specific for each system and are given in Table 3 in the altitude entry. Since the LEO orbits analyzed are circular, the apogee and perigee altitude values are equal.
Argument of perigee	The angle, in the plane of the satellite's orbit, between the ascending node and the perigee of the orbit, measured in the direction of the satellite's motion. This parameter is set to zero for circular orbits.
Right ascension of the ascending node (RAAN):	The RAAN is the angle in the Earth's equatorial plane measured eastward from the vernal equinox to the ascending node of the orbit, where the ascending node is the point in the satellite's orbit where the Earth's equatorial plane going from north to south is crossed. In this analysis, the RAAN of the first orbit plane is set to zero as a reference. The RAAN of the other planes are made equal to multiple of the plane spacing, as defined in Table 3. Adjacent planes are located on either side of the reference plane.
Mean anomaly:	The mean anomaly is the angle, in the satellite orbital plane, between the perigee of the orbit and the position where the satellite would be if it always moved at its average angular rate. In this analysis, the mean anomaly of the reference satellite is set to zero. The anomaly for the other satellites is equal to 360° divided by the number of satellites in the plane plus the plane phasing, as defined in Table 3, corresponding to the plane in which the satellite is located.
Plane phasing	Offset angle in the distribution of satellites in each plane, in relation with the first plane.

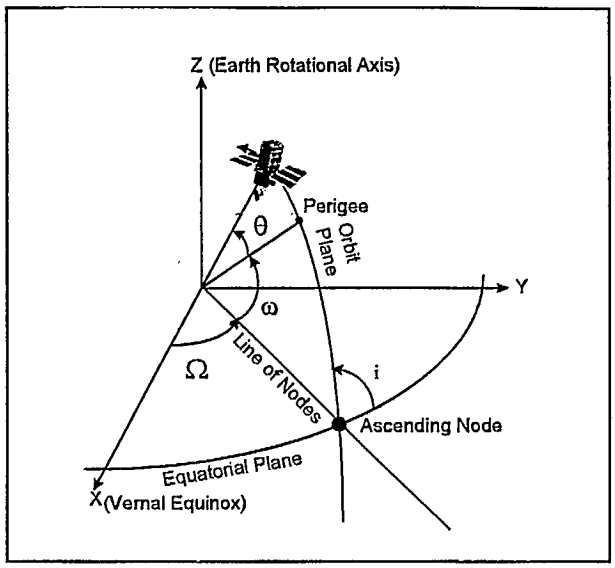

Figure 1 Orbital geometry parameters

3.2 Case Study: Teledesic

The Teledesic system is to provide global multi-media links via a constellation of 288 LEO spacecraft organized in 12 orbital planes of 24 satellites each. Each satellite is to be linked with eight of its neighboring spacecraft. Four of these links will be with satellites in the same orbital plane, two forward and two backward. The other four will be with satellites in adjacent planes: one on each of the four closest adjacent planes.

There are two case studies for the Teledesic constellation. One, as represented by Figure 2, where the satellites in adjacent planes travel in the same direction, and another case, as represented by Figure 3, where the satellites travels in opposite directions. The case represented by Figure 3 occurs around the "seam" where the first and last orbital planes run side-by-side but in opposite direction. The interaction at the seam is of concern for the first two and last two orbital planes only.

Table 5 gives the parameters used to simulate the Teledesic orbital characteristics with the STK software. Note that since in Teledesic, the orbits are located in different altitudes (0.5 km of separation between them), the plane phasing is constantly changing. In Figure 2, a disposition is given at random.

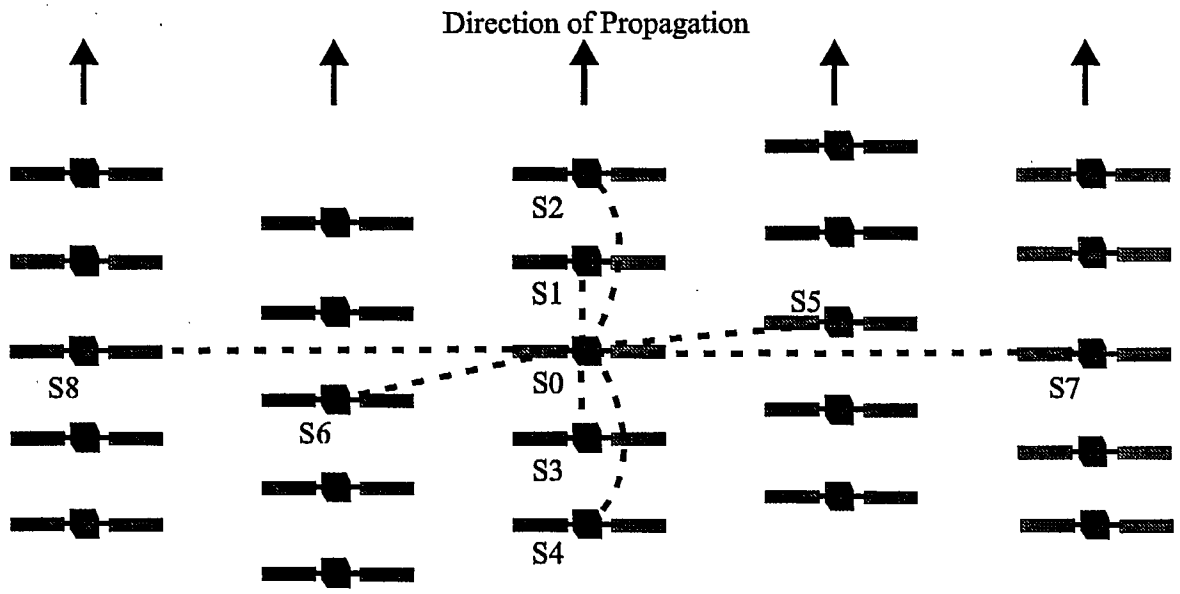

Figure 2 Teledesic regular ISL link configuration. Each satellite is linked with eight of its neighbouring satellites, located in the same plane and in adjacent planes. The links of only one satellite is shown here for clarity.

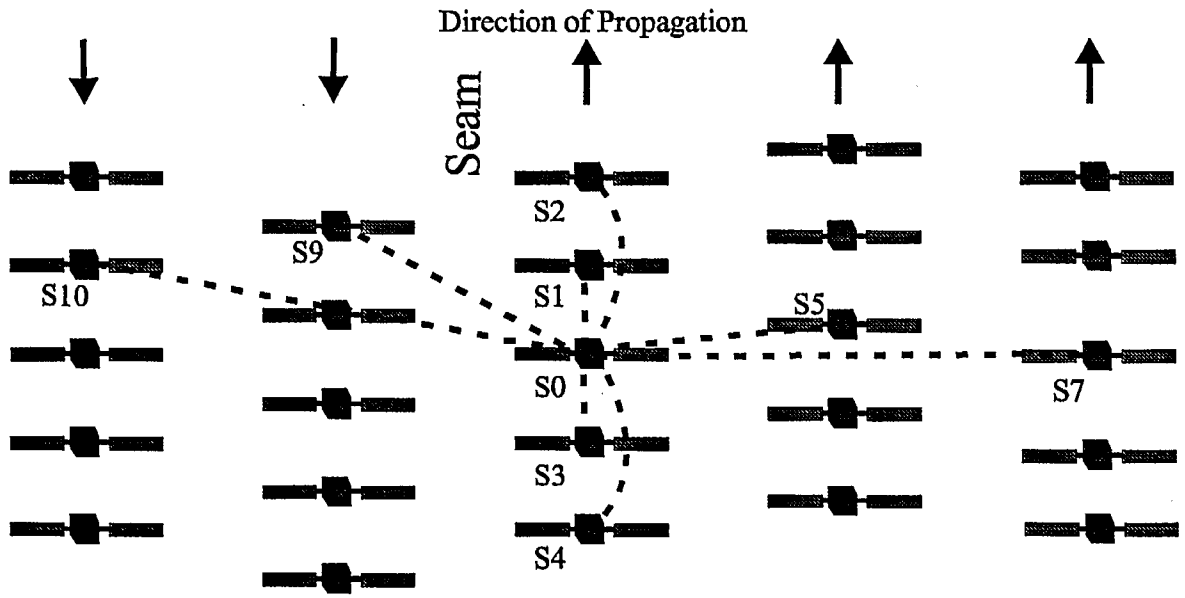

Figure 3 Teledesic ISL link configuration at the seam. Satellites in the S0 orbital plane run parallel but in opposite direction of satellites in the S9 and S10 orbits. Each satellite is still linked with eight of its neighbouring satellites, located in the same plane and in adjacent planes.

Table 5 - System parameters for Teledesic

Altitude	1350 km
Inclination	90 degrees
Number of planes	12
Number of satellites per plane	24
Plane spacing	15 degrees
Plane phasing	Random
Crosslinks	With 8 adjacent satellites: 2 preceding and 2 following in same orbital plane, 1 on each of the 4 closest adjacent planes

3.2.1 Teledesic – Regular Link Analysis

Figure 4gives a pictorial representation of the Teledesic constellation used for the regular (i.e. not at the seam) link simulation. It is based on the diagram shown in Figure 2. Satellite S0 is chosen as the reference payload. It is initially positioned at the equator at 100° west of longitude. As described in Table 5, S0 is in communications with its 8 neighbors, S1 to S8. Each satellite on a specific orbit is separated from its adjacent one by 15° and each orbit is separated from its adjacent one also by 15° (plane spacing). Therefore, satellites S1 and S2, which lead S0 on the same orbit, are spaced, from S0, by 15° and 30° respectively, while S3 and S4, which lag S0, are located at -15° and -30° on the S0 orbit. S5 and S6 are on the immediate adjacent orbital plane, ±15° from the S0 orbit, while S7 and S8 are on the next one over at ±30°.

Since adjacent orbits are separated by 0.5 km in altitude, the relative position between satellites on different orbits (plane phasing) is drifting. Therefore, the constellation arrangement depicted by Figure 4 is only a special case for the simulation. For a complete simulation, one must consider all possible plane phasing, from –7.5° to +7.5°. Beyond that range, a satellite would be linked to the next satellite.

From the simulations, it is seen that all eight communications links can be maintained at all time. However, this would create real challenging requirements for the azimuth and elevation steering mechanisms. The elevation steering mechanism would be required to scan between ±90°, and the azimuth would need to be scanning over a complete 360 °. This would be needed to allow cross over of the satellites at the poles. However, those requirements can be reduced significantly if one is to limit communications links for when the satellites are inside ±85 ° of latitude.

Table 6 shows the simulation results for links established between S0 and the other eight satellites between ±85 ° of latitude, i.e. whenever one satellite goes over the limit, the link is broken. Figure 5 and Figure 6 display graphically the values of azimuth, elevation, range and their rate of change as a function of time for the interaction between S0 and S5 (adjacent orbits) and S0 and S7 (two orbits apart) respectively. Graphs similar to those shown in Figure 5 and Figure 6 could be produced for S6 and S8 but with the azimuth centered on 270° instead of 0° since the orbits are on the other side.

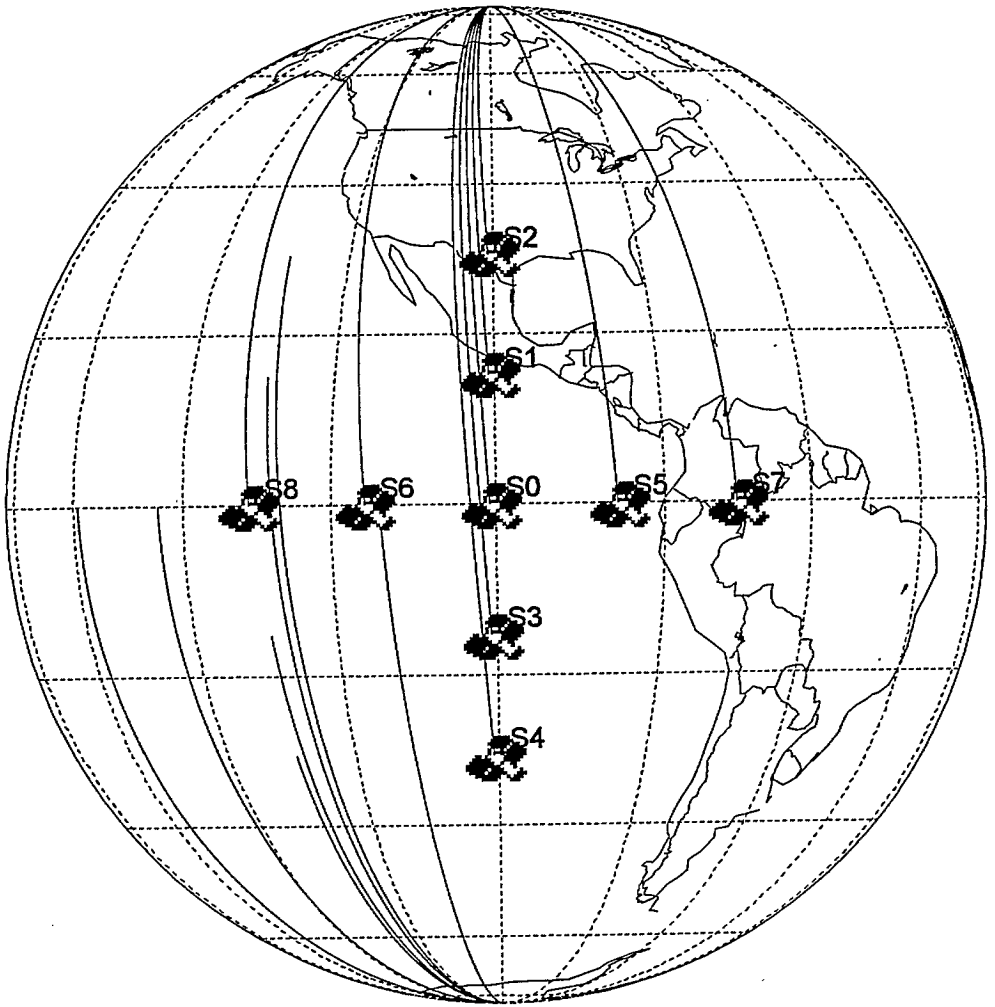

Figure 4 Satellites distribution for Teledesic case study simulation.

Table 6 Orbital interaction between satellite S0 and its 8 neighbors, as defined in Table 5 and Figure 4 for Teledesic, for satellites travelling between ±85o of latitude.

		Satellite							
		1	2	3	4	5	6	7	8
Azimuth [degrees]		0	180	0	180	±81	±81	±73	±73
Azimuth rate [°/minute] Tracking Re-Acquisition		0	0	0	0	6 40	6 40	10 50	10 50
Elevation [degrees]		-7.5	-15	-7.5	-15	±5°	±5°	±8°	±8°
Elevation rate [°/minute] Tracking Reacquisition		0	0	0	0	0.6 2	0.6 2	1 2	1 2
Range [km]	Min	2017	403	2017	4034	175	175	348	348
	Max		4			2254	2254	4119	4119
Range rate [km/minute]		0	0	0	0	115	115	170	170
Period for which link is maintained (min)		A	A	A	A	51 to 53	51 to 53	51 to 53	51 to 53
Period for Link broken (min)		0	0	0	0	3 to 6	3 to 6	3 to 6	3 to 6

Note: "A" means Always, i.e. the link is always maintained.

Satellites on the same orbit (S0, S1, S2, S3, S4) are seen stationary from one to another. The azimuth, elevation and range do not vary. This is not the case for satellites on different orbits. The azimuth, elevation and range values entered in Table 6 are the extremes. The last two rows of entries indicate the duration for which the links between satellites can be maintained continuously and the duration for which the links are broken, at the poles. For links established within an orbit, no breakage occurs. For inter-orbit links, the communications can be established for 51 to 53 minutes, depending on the relative positions of the satellites. The links are then broken for 3 to 5 minutes before reacquisition must be done.

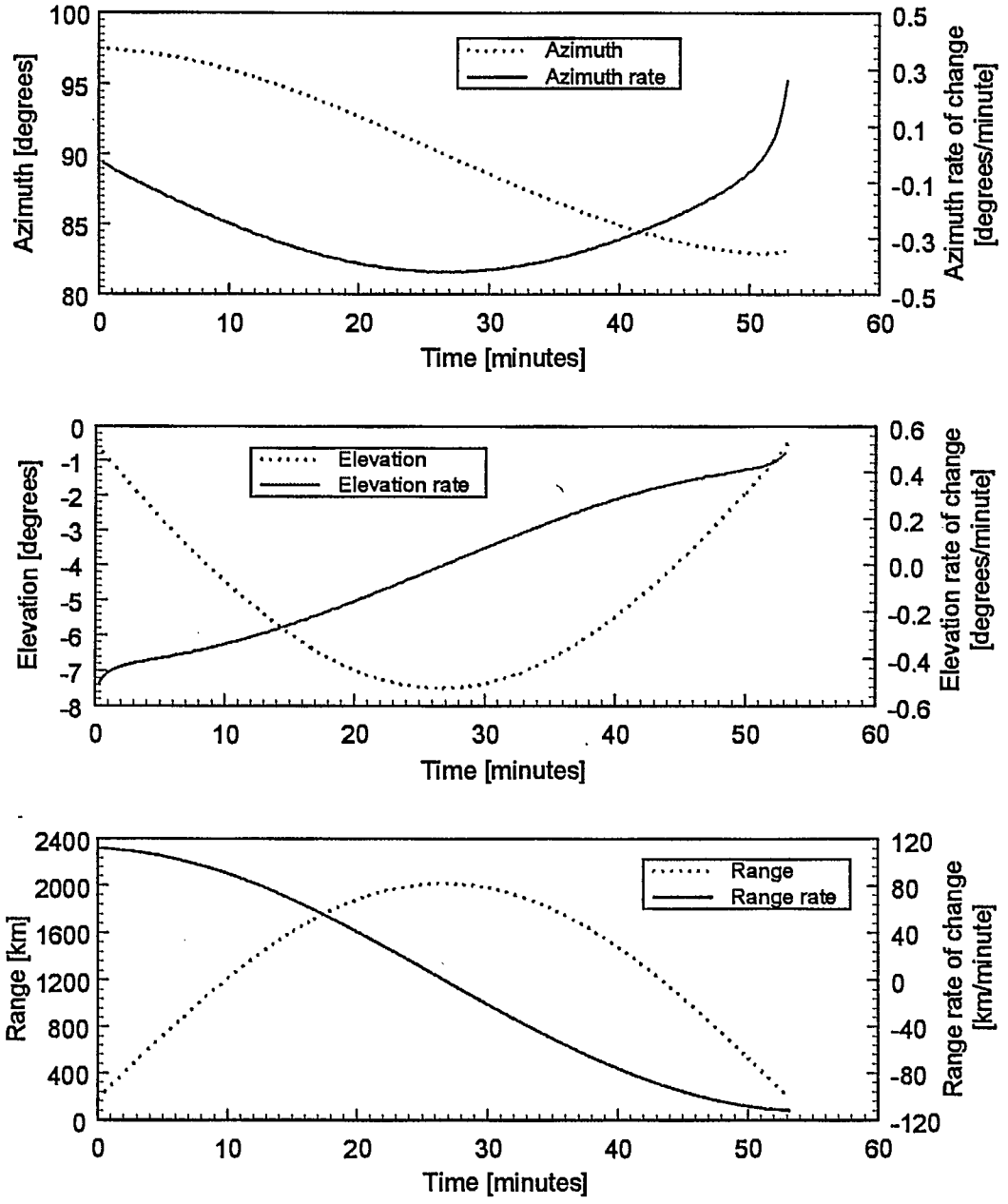

Figure 5 - Azimuth, elevation, range and their rate of change as a function of time for a Teledesic regular link between two satellites located on adjacent planes with initial plane phasing of 0 degree (S0 and S5 on Figure 4).

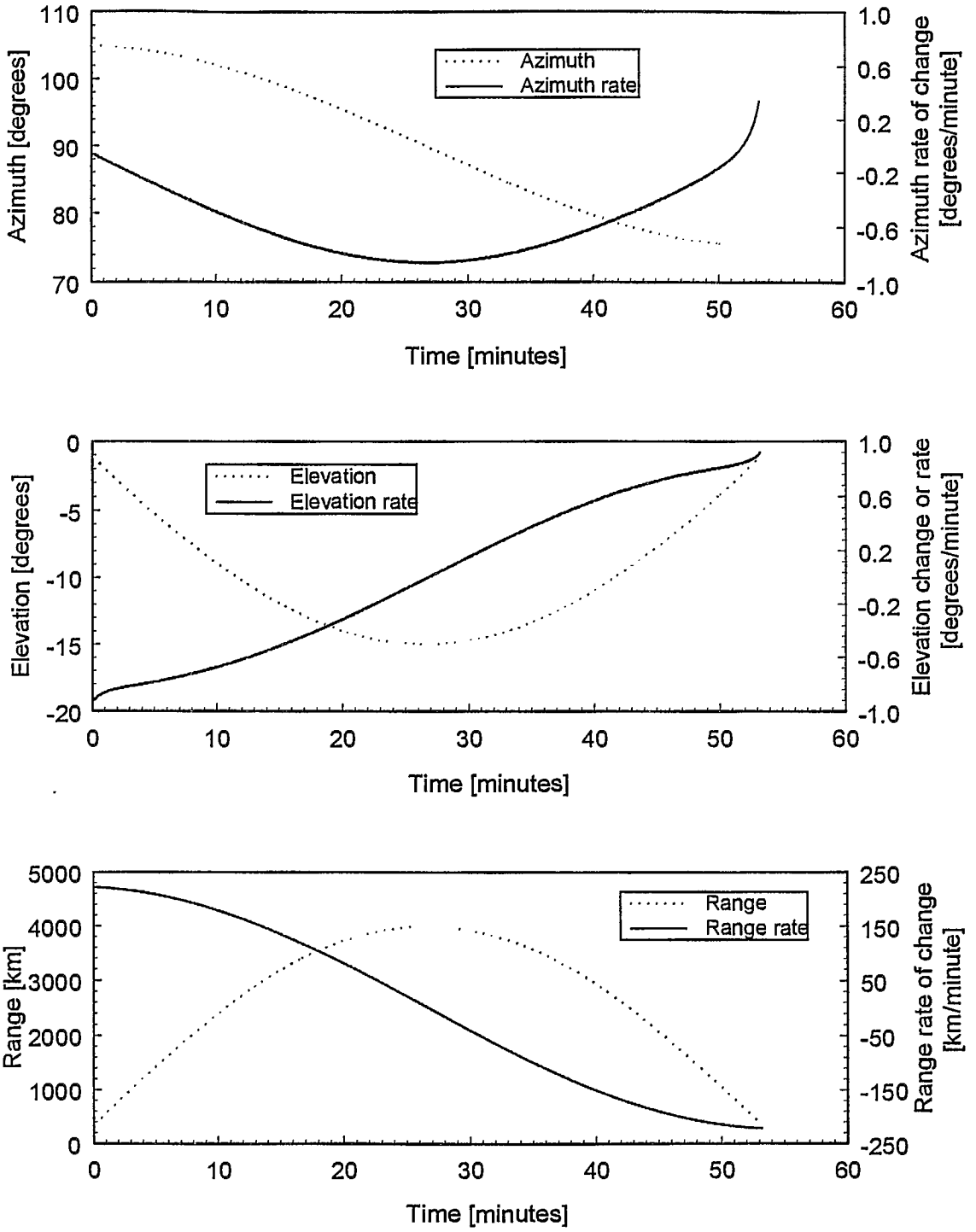

Figure 6 Azimuth, elevation, range and their rate of change as a function of time for a Teledesic regular link between two satellites located on two orbital planes apart with initial plane phasing of 0 degree (S0 and S7 on Figure 4).

3.2.2 Teledesic - interaction of satellites at the seam

As mentioned earlier, at the orbital seam, (Figure 3), the satellites on adjacent planes travel in opposite directions and the rate of change of the orbital parameters increases significantly.

The orbital simulation, described in this section, is based on the diagram shown in Figure 3. Satellite S0 is chosen as the reference payload. It is initially positioned at the equator at 100° west of longitude. S0 is linked with S9 located on the first orbit across the link (orbit 12 of the constellation) and with S10 located on the second orbit across the link (orbit 11 of the constellation). Orbit 11 is at an altitude of 5 km higher than orbit 1 and orbit 12 at 5.5 km higher. Again, because satellites on different orbits are drifting relative to each other, multiple simulations must be done to cover the extreme cases.

Figure 7 shows a graphical representation of the simulation results for links established across the seam between S0 and every satellites on the S10 orbit (each dotted line represents a distinct link) for azimuth, elevation and range parameters. The dark lines show how the links should be restricted to maintain the azimuth, elevation and range values within the limits of regular links as defined in Table 6. In those cases, it is seen that links are established between every fourth satellites.

As expected, the link duration and the rate of change are modified considerably. From the simulations, it is found that links, between two satellites on adjacent orbits, can be established for approximately 21 minutes and for 8.5 minutes for links across two orbits. However, the link range would reach 8700 km. This is approximately twice the maximum link range of the regular orbits defined in section 3.2.1. Communications along that link distance would require a 6 dB increase in optical power or that the diameter of the telescope aperture be doubled.

To simplify the terminal design, it is suggested that the azimuth, elevation and range requirements be restricted to values similar to those of a regular link as described in Table 6. This would however considerably reduce the period of time for which links can be maintained, but at the benefit of much a simpler system. Table 7 tabulates the results of the restricted links in a format similar to the one of Table 6.

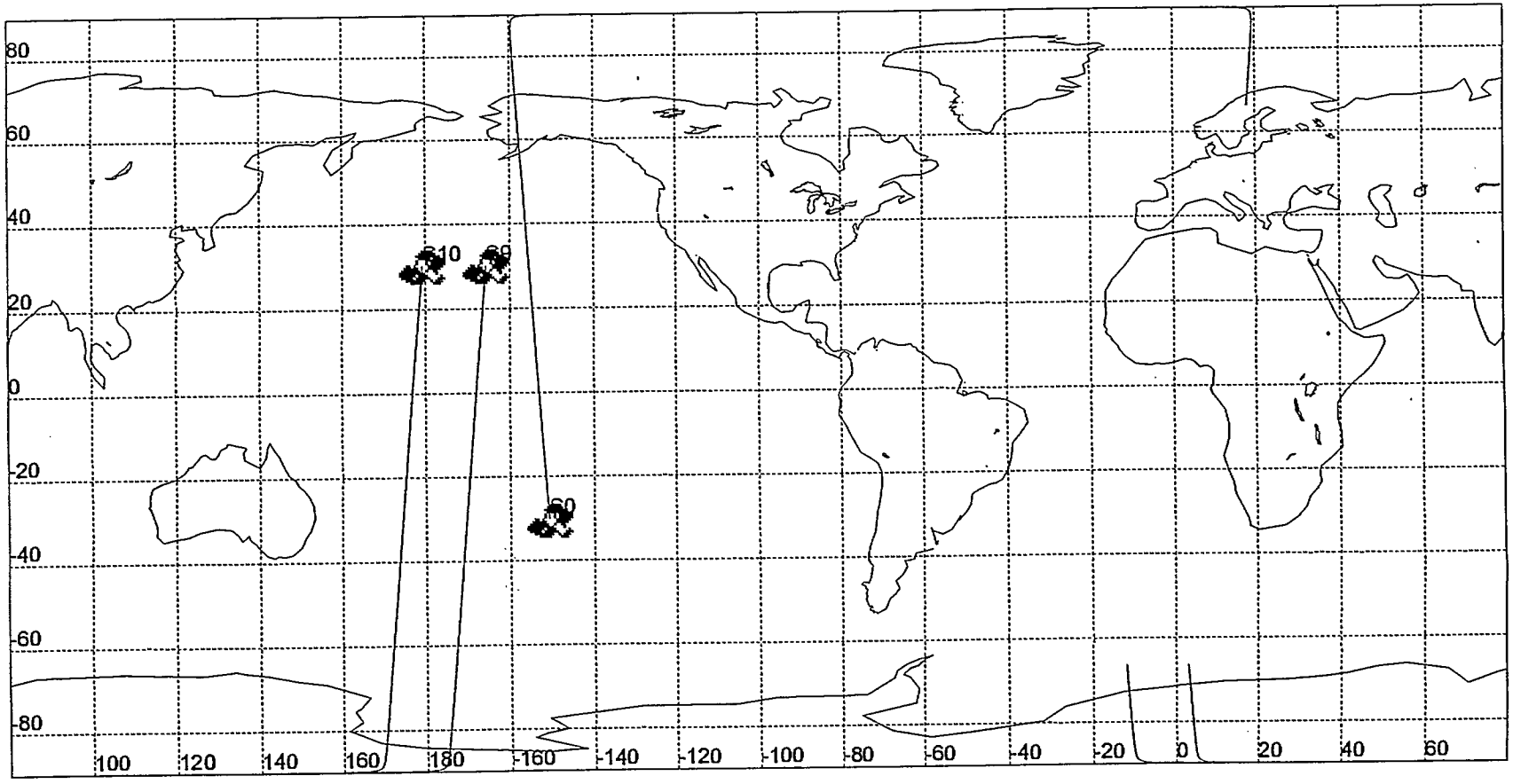

Figure 7 Satellite distribution for Teledesic at the seam.

Table 7 Orbital interaction parameters between satellite S0 and its neighbours across the seam as defined in Table 5 and for Teledesic. The values entered are for link range smaller than 4200 km and for satellites within ±85° of latitude.

		Satellites	
		9	10
Azimuth [degrees]		±80	±80
Azimuth rate (max)		15°/min	15°/min
Elevation [degrees]		±15°	±15°
Elevation rate (max)		3°/min	2°/min
Range[km]	Min	350	350
	Max	4200	4200
Range rate [km/sec]		10	12
Period for Link maintained (min)		9	3 to 10

3.2.3 Teledesic System Requirement Summary

Table 8 gives a summary of the system requirements. The last two entries relate to the speed at which the telescope must be swung around during communications outage to reacquire the next satellite. The values of the last two entries were found in the literature.

Table 8 Teledesic system requirements summary

1	Data Rate	2.5 Gbps
2	Bit Error Rate	10^{-6}
3	Minimum Range	150 km
4	Maximum Range	4200 km
5	Maximum Latitude	±85°
6	Scanning range (Azimuth)	±110°
7	Scanning range (Elevation)	±15°
8	Max. Scan Rate (Azimuth) Tracking Re-Acquisition	15°/min
9	Max. Scan Rate (Elevation) Tracking Re-Acquisition	2°/min
10	Azimuth slew rate	6°/sec
11	Elevation slew rate	6°/sec

3.3 Case Study: Celestri

In this section, the Celestri project, from Motorola, is analyzed. As mentioned in Table 3, Celestri is a hybrid system composed of both LEO and GEO satellites. The LEO satellites will provide real-time interactive bandwidth-on-demand applications while the GEO satellites will be used for broadcast and multicast applications. Only the LEO satellites will be equipped with ISL capability. The following sections will therefore study only the LEO-LEO ISL.

3.3.1 Constellation Description

The LEO constellation is divided in 7 orbital planes of 9 satellites each. Each satellite is to be linked with six of its neighbouring spacecraft as shown in Figure 8. Two of these links will be with satellites in the same orbital plane, one forward and one backward. The other four will be with satellites in adjacent planes: two on each of the two adjacent planes. In Celestri, the plane phasing can be maintained constant at 28.57°. **Table 9** gives the parameters used to simulate the Celestri orbital characteristics with the STK software.

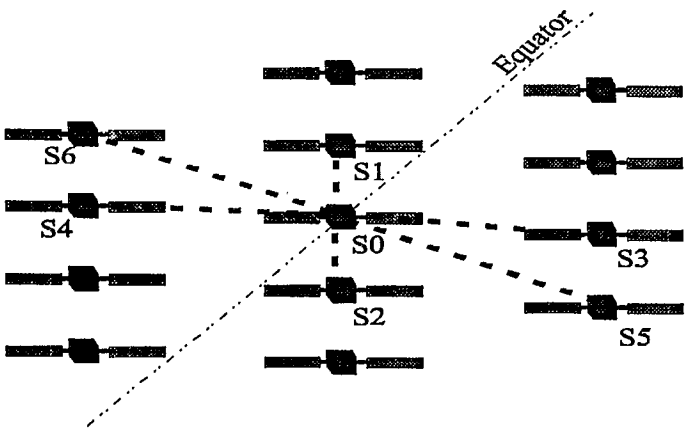

Figure 8 Celestri ISL link configuration. Each satellite is linked with six of its neighbouring satellites, located in the same plane and in adjacent planes. Satellites located on the same plane are spaced by 40°; planes are spaced by 51.43° and offset by 28.57°. The links of only one satellite, S0, is shown here for clarity.

Table 9 System parameters for Celestri

Altitude	1400 km
Inclination	48 degrees
Number of planes	7
Number of satellites per plane	9
Plane spacing	51.43 degrees
Plane phasing	28.57 degrees
Crosslink	With 6 adjacent nodes in the same plane and other planes

Figure 10 gives a pictorial representation of the constellation used for the orbital simulation. Satellite S0_0 is chosen as the reference payload. Similar to the previous simulation, it is initially positioned at the equator, at 100° W. It is in communications with six of its neighbors. On the same orbit, the satellites S0_1 and S0_2 are spaced by 40° on each side of S0_0. Satellites S1_0 and S7_0 are located on the adjacent planes at ±51.43° from the reference plane and are offset by ±11.43° on the orbit. Satellites S1_1 and S7_1 are also located on the adjacent plane, at ±51.43°, but are offset by ±51.43°.

3.3.2 Celestri – Link Analysis

A complete orbit for a Celestri satellite requires 1 hour 53 minutes and 45 seconds. The results of the simulation are tabulated in Table 11. Graphical representations of the azimuth, elevation, range and the rate of change for the S1_0 and S1_1 links are shown in Figure 11 and Figure 12. The results for the link between S7_0 and S7_1 would be the same except for the fact that the azimuth angle would be negative.

From inspection of the results, the following conclusions can be reached:

- The simulations showed that every satellite could have a continuous link to its six adjacent satellites.
- Due to the inclination of the orbits, communications across the seam is not required for Celestri.
- As with Teledesic, satellites on similar orbits are seen stationary in relation to each other.
- Only two satellites are accessible at all time from a satellite on an adjacent orbital plane.
- The minimum range, between two satellites is 2000 km and the maximum is at 5900 km.
- In order to maintain communications for a complete orbit without switching to another satellite, the telescope must cover a maximum excursion of ±75° in azimuth and ±7° in elevation.

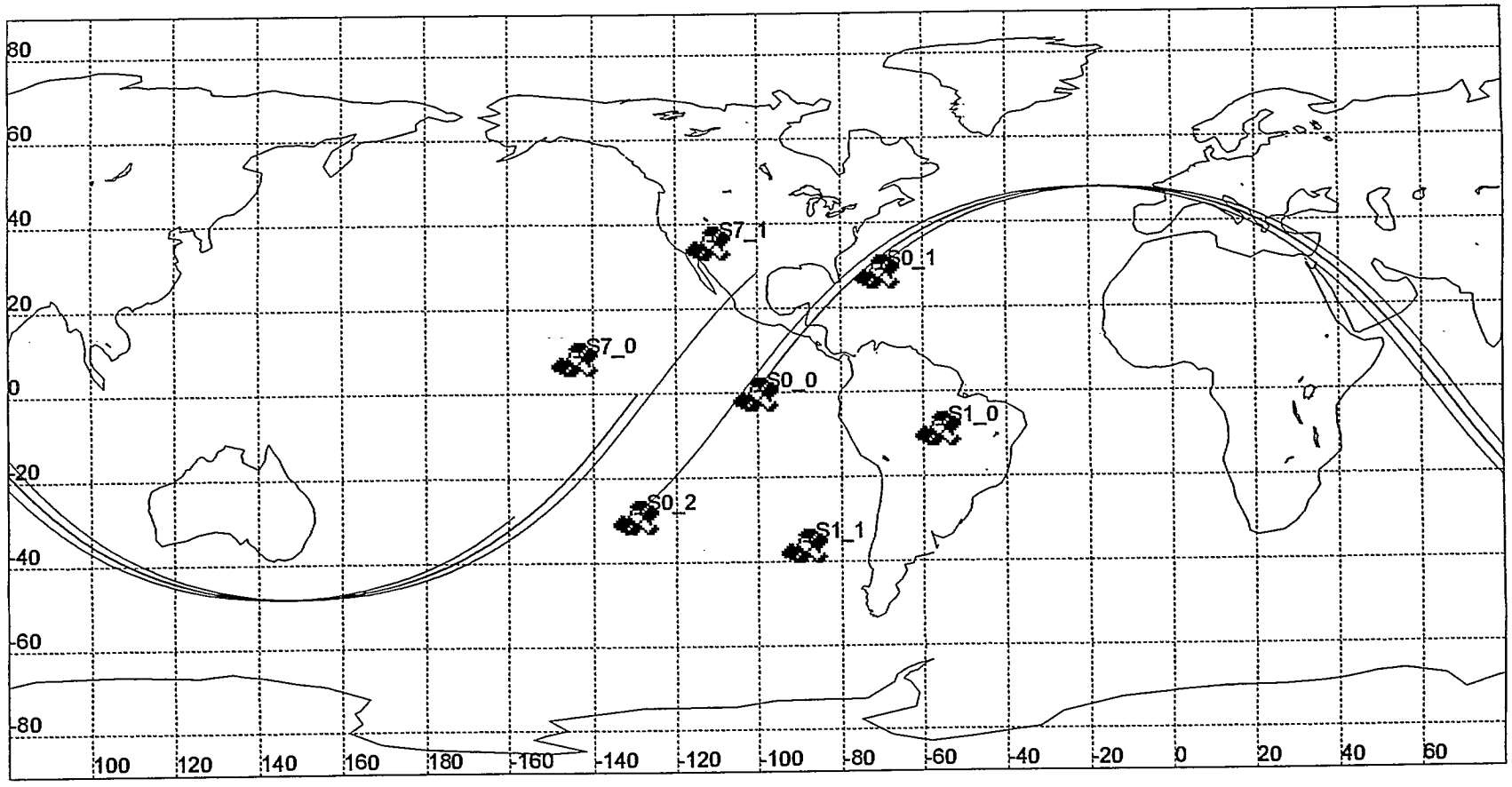

Figure 9 Satellite relationship for Celestri simulations.

Table 10 Orbital interaction between satellite S0 and its 6 neighbours, as defined in Figure 9 and Table 10 for Celestri.

		Satellite Number					
		S0_1	S0_2	S1_0	S7_0	S1_1	S7_1
Azimuth [degrees]		0	180	±65	±65	±75	±75
Azimuth rate [°/minute]		0	0	5.1	5.1	7.9	7.9
Elevation [degrees]		-20	-20	±6°	±6°	±7°	±7°
Elevation rate [°/minute]		0	0	0.6	0.6	0.7	0.7
Range [km]	Min	5320	5320	3100	3100	2000	2000
	Max			5900	5900	5400	5400
Range rate [km/minute]		0	0	155	155	187	187

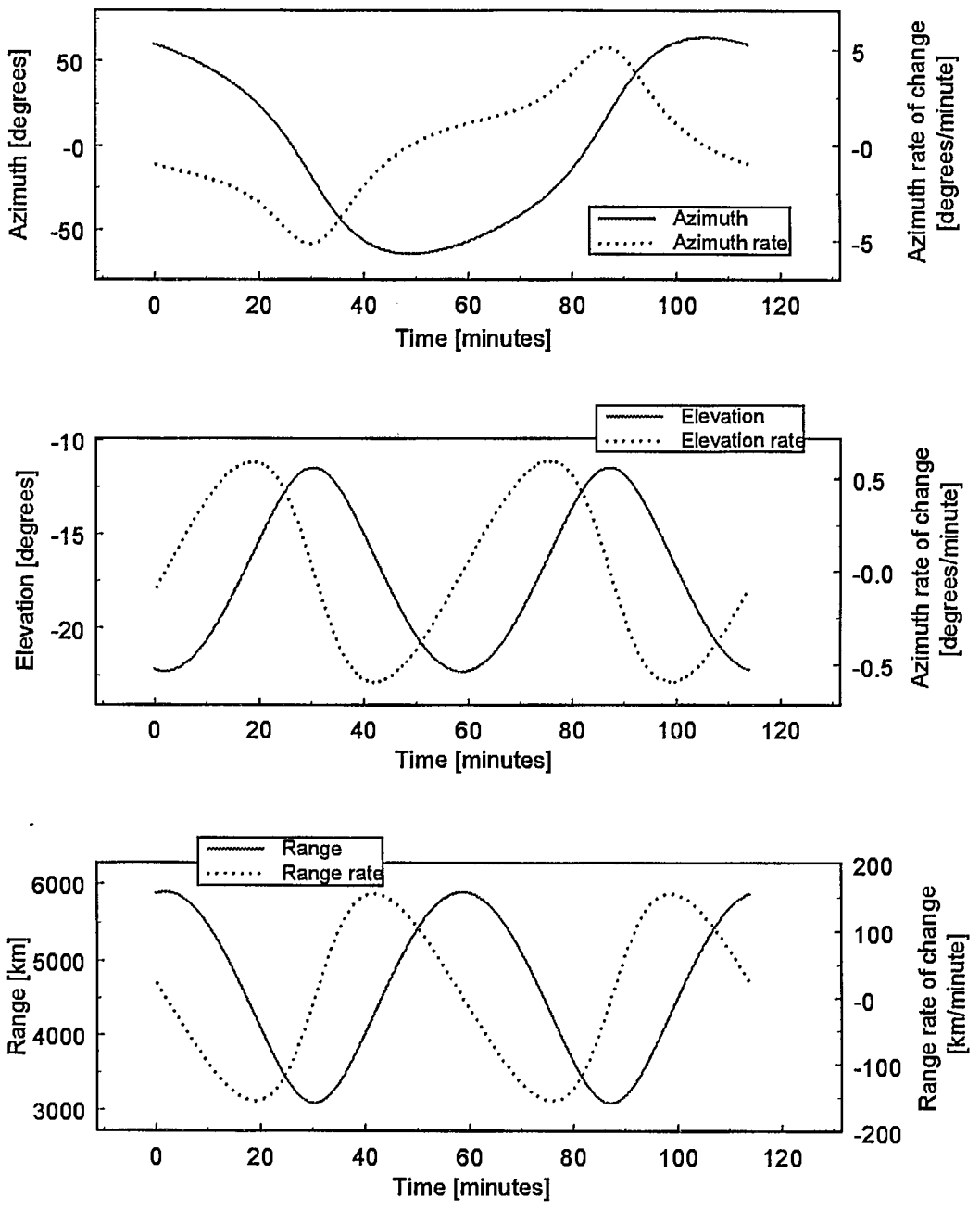

Figure 10 Celestri link parameters for S0_0 to S1_0 link.

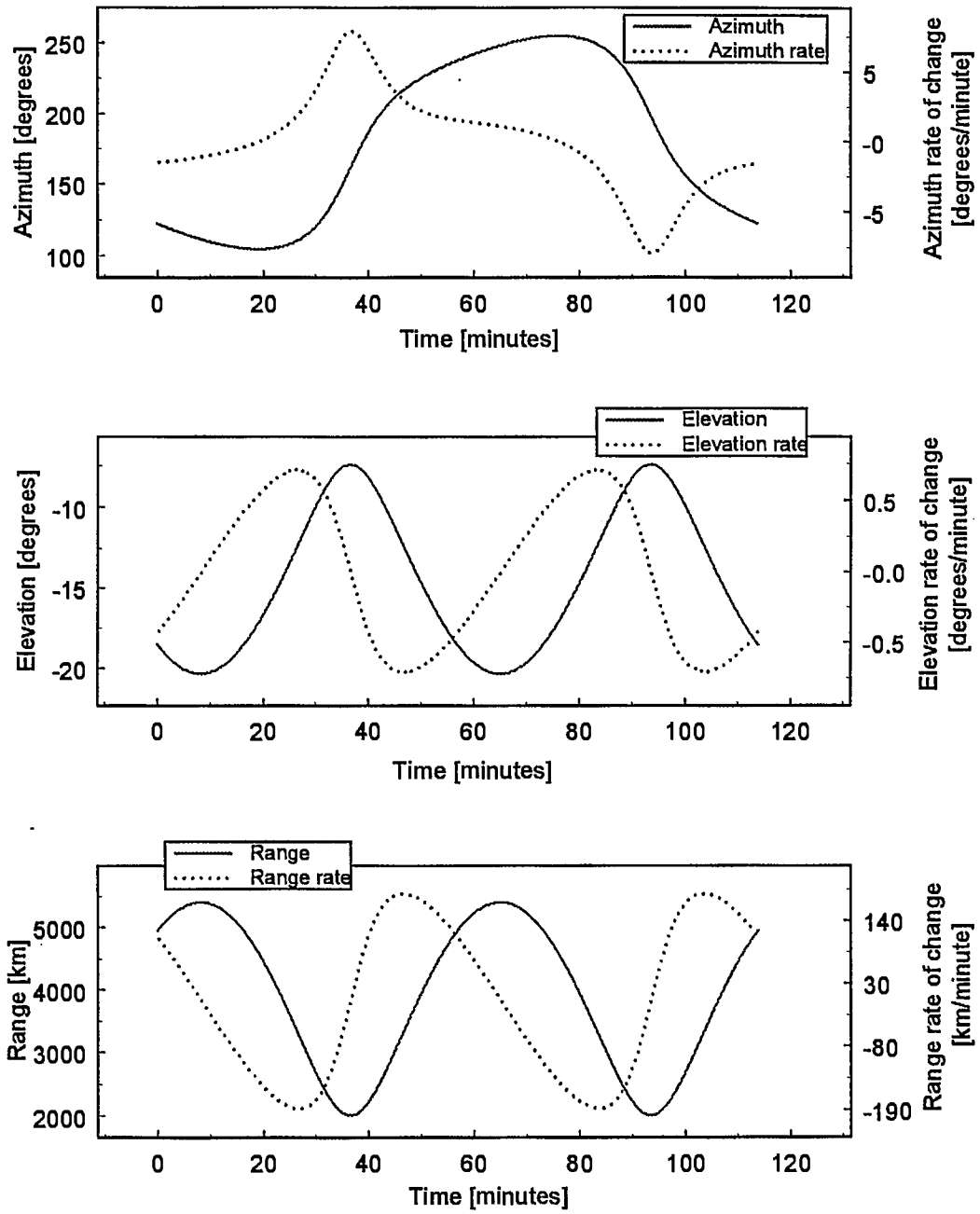

Figure 11 Celestri link parameters for S0_0 to S1_1 link.

3.4 Doppler Shift

When two satellites move away from each other or towards each other while trying to communicate, a Doppler shift affects the frequency of the intersatellite link signal. The range rate of change creates a Doppler shift according to the following equation:

$$f` = f \frac{1 - \frac{u}{c}}{\sqrt{1 - \left(\frac{u}{c}\right)^2}}$$

where

f' is the Doppler shifted frequency;
f is the frequency of operation,;
u is the relative velocity between the two platforms;
c is the speed of light.

Figure 12 shows a graphical representation of the Doppler shift, in MHz, for the three cases studied, Teledesic regular, Teledesic seam and Celestri. For Celestri and the regular Teledesic links, Doppler shift up to 2 GHz occurs. For Teledesic, at the seam, the optical frequency may vary from ±9GHz in the five minutes the link is established. Table 11 tabulates the maximum values of Figure 12. These values assume a nominal optical wavelength of 1550 nm.

	Doppler shift [MHz]
Celestri	2015
Teledesic	1884
Teledesic-seam	8958

Table 11 - Doppler shift comparison for seam and non-seam cases

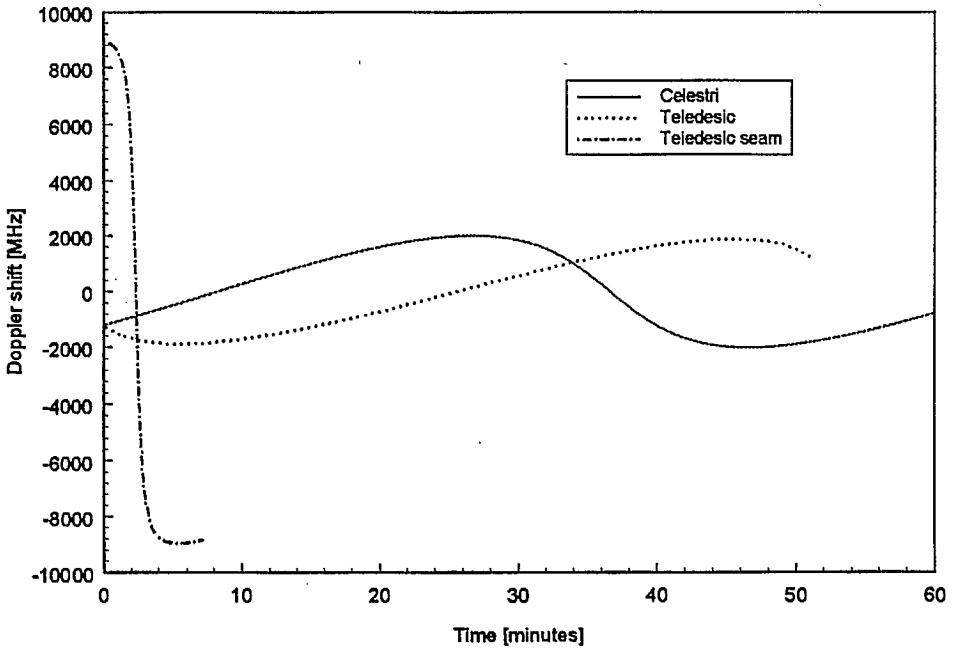

Figure 12 Doppler shift for the seam of Celestri and Teledesic

4. LINK PERFORMANCE ANALYSIS

In this chapter, the performance of optical intersatellite links, expressed in terms of bit-error probability, will be defined. Equations will be derived and graphs plotted to show the effect of various parameters such as transmit power level, antenna diameter, link range, noise sources, and modulation schemes. In the first section, the optical power budget will be defined and an equation to evaluate the detected power will be derived. In the second section, an analysis of the noise contribution will be done. In the last section, the detected power level and the noise level will be combined and bit error rate curves for various modulation formats will be presented. It is assumed, in this analysis, that the two platforms have achieved acquisition and that tracking is maintained.

4.1 Optical Power Budget

The optical power received at the photodetector, P_{opt_rx}, can be expressed as:

$$P_{opt\_rx} = (P_L G_{tx\_opt\_amp} G_{tx\_tel} L_{tx\_wf} L_{tx\_opt} L_{tx\_pt}) * L_r * (G_{rx\_tel} L_{rx\_opt} L_{rx\_pt} G_{rx\_opt\_amp}) \quad (1)$$

where

P_L = Optical power of the source,
$G_{tx\_opt\_amp}$, $G_{rx\_opt\_amp}$, = Transmitter and receiver optical amplifier gain,
G_{tx_tel} , G_{rx_tel} = Gain of the transmitting / receiving telescope,
L_{tx_wf} = Loss due to wavefront errors,
L_{tx_opt} , L_{rx_opt} = Loss due to transmit/receive optics transmissivity,
L_r = Range loss,
L_{rx_pt} = Pointing loss,

4.1.1 Telescope gain ($G_{tx\_opt\_amp}$, $G_{rx\_opt\_amp}$)

The classical telescope gain formula is written for an ideal, uniformly illuminated circular aperture of diameter D as [13]:

$$G(\theta) = \left(\frac{\pi D}{\lambda}\right)^2 * \left(\frac{2 J_1(\pi \sin\theta)}{\pi \sin\theta}\right) \quad (2)$$

Where λ is the optical wavelength, θ the angular displacement and $J_1(x)$ the Bessel function of the first order. For on-axis gain (θ=0), the gain formula simplifies to the well known expression:

$$G(\theta) = \left(\frac{\pi D}{\lambda}\right)^2 \quad (3)$$

However, in laser communications, the near-field profile of the transmitted beam is Gaussian or nearly Gaussian, with an amplitude plane wave with a waist size ω_0 impinging onto a circular aperture D_{aper} with an obscuration D_{obs}. In those cases, the gain of the transmit antenna is reduced and can be expressed as [14]:

$$G_{tx}(\theta) = \left(\frac{\pi D}{\lambda^2}\right)^2 2\alpha^2 \left(\int_{\gamma^2}^{1} \exp(-\alpha^2 u) J_0(X(\theta)\sqrt{u})\, du\right)^2 \quad (4)$$

where

$$\gamma = \frac{D_{obs}}{D_{aper}} \qquad \alpha = \frac{D_{aper}}{2\omega_0} \qquad X(\theta) = \frac{2\pi}{\lambda} D_{aper} \sin(\theta)$$

Note that the central obscuration creates a need to optimize the trade-off between α and γ in an effort to maximize the net power being passed through that annular aperture. Klein and Degnan [14] have derived a simple approximation exact at $\gamma = 0$ and accurate to within ±1% for γ <0.4.

$$\alpha_{optimum} = 1.12 - 1.3\,\gamma^2 + 2.12\,\gamma^4 \quad (5)$$

For the receive antenna, the incoming field can be approximated as uniform and therefore the gain equation corresponds to the usual equation $(\pi D / \lambda)^2$. If the effect of obscuration from the central mirror and supports are taken into effect as well as various losses at the detector such as fractional signal power detected, the receiving antenna gain can be written, for direct detection, as [15]:

$$G_{rx} = \left(\frac{\pi D}{\lambda^2}\right)^2 (1 - \gamma^2)\,\xi \quad (6)$$

where

$$\xi = \frac{2}{(1-\gamma^2)} \left(\int_0^{\frac{2\pi D}{\lambda 4F}} \frac{(J_1(u) - \gamma J_1(\gamma u))^2}{u} du \right) \quad (7)$$

and F being the F-number of the telescope.

4.1.2 Wavefront error losses ($L_{tx\ wf}$)

The wavefront loss is associated with aberrations of the optical signal by the optical elements in the transmit path. An rms quantification of these error contribution is typically used to determine the loss due to wavefront error and is expressed as $\sigma = \lambda/x$ where x is in the order of 10 for most laser communications systems. The wavefront error loss can be computed by:

$$L_{tx\_wf} = e^{-\left(\frac{2\pi\sigma_{rms}}{\lambda}\right)^2} \quad (8)$$

When a number of optical surfaces are involved, the net overall σ_{rms} can be determined by:

$$\sigma_{rms1} = \sqrt{\sigma_1^2 + \sigma_2^2 + \ldots + \sigma_n^2} \qquad (9)$$

Typical values for optical element quality are:

Flat mirrors and plates (<4")	λ/200	Spherical mirrors (<14")	λ/40
Flat mirrors and plates (4 - 14")	λ/50	Spherical lenses (<14")	λ/40
Cube beamsplitters	λ/20		

4.1.3 Transmission loss (L_{tx_opt}, L_{rx_opt})

Transmission loss is caused by the optical lenses and coatings in the optical network, which have finite transmissivity at the desired wavelength. For a typical OISL system containing 1 thermal window, 1 primary mirror, 1 secondary mirror, ≅10 lenses in the eye piece, 1-2 fine pointing mirrors, 3-4 beam splitters, 3-4 lenses at the laser or detector, the transmissivity would be on the order of 80%.

4.1.4 Propagation loss (L_r)

The propagation loss, resulting from the diverging wavefront of the optical signal as it propagates the link distance, R, can be expressed by the classical expression:

$$L_r = \left(\frac{\lambda}{4 \pi R} \right)^2 \qquad (10)$$

4.1.5 Link Gain G_{link})

From the above definitions, the gain of the link can be computed using the expression:

$$G_{link} = \frac{P_{opt\_rx}}{P_L * G_{tx\_opt\_amp} * G_{rx\_opt\_amp}} \qquad (11)$$

$$= (G_{tx\_tel} L_{tx\_wf} L_{tx\_opt} L_{tx\_pt}) * L_r * (G_{rx\_tel} L_{rx\_opt} L_{rx\_pt})$$

From Eqn 11, one can write the optical power impinging on the photodetector as:

$$P_{opt\_rx} = P_L * G_{link} * G_{tx\_opt\_amp} * G_{rx\_opt\_amp} \qquad (12)$$

These equations can be used to analyze the effect changes in the various parameters have on the link. Using the baseline parameters defined in Table 12, Figure 13 shows the variation of the link gain, (G_{link}), for various antenna diameters ($D_{tx} = D_{rx}$) and various range links (R).

Table 12 Link Parameters

Optical wavelength	λ	1550 nm
Ratio of central obscuration over antenna diameter (γ)	$\frac{D_{obx}}{D_{aper}}$	0.2
Tx / Rx wavefront loss	$L_{tx\ wf}$	1.7 dB
Tx / Rx transmissivity loss	$L_{tx\ opt}$	0.97 dB
Transmitter pointing error	θ	1 μrad

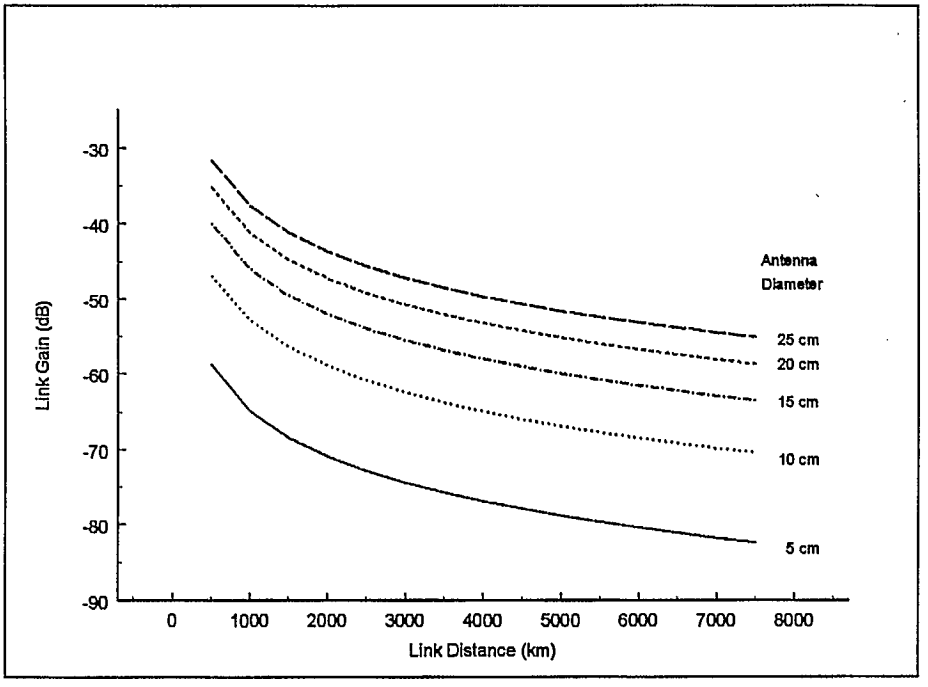

Figure 13 Link gain as a function of free space distance between the two platforms for various antenna diameters. The other system parameters are defined in Table 12 .

4.2 Noise analysis

In order the minimize the transmission error probability, it is important to maximize the signal-to-noise ratio (SNR). In this section, the most important noise sources will be described and equations will be derived to evaluate noise power spectral density (in A^2/Hz) produced by each one. The noise sources to be considered are:

- Shot noise,
- Dark current noise,
- Thermal noise,
- Circuit noise,

4.2.1 Shot noise

Since the photo-detection of the incoming photons is a statistical process, it introduces shot noise proportional to the dc-current in the photodiode, with a uniform one-sided power spectral density equal to:

$$i_{SN}^2 = 2\,q\,F\,P_{opt}\,\eta_d\,M^2 \qquad (13)$$

where

- q is the electronic charge,
- F the detector excess noise factor,
- P_{opt} is the detected optical power from the desired signal P_{sig}, the background sources, P_b, and the local oscillator P_{LO} (if heterodyne detection is used),
- η_d the detector sensitivity (A/W),
- M the detector gain,
- B_{rf} the RF bandwidth.

4.2.2 Excess Noise Factor

The excess noise factor, F, present in some photo-detectors such as in avalanche photodiodes, is a results of the multiplication process of photo-generated electrons. Due to the statistical nature of multiplication process, every photo-generated electron undergoes a different gain, with a fairly broad non-Gaussian probability distribution. As a result, the magnitude of the multiplied detector noise is increased by a factor F over what it would be in a perfect, noiseless detector. F has been shown to be a function of the average gain M and a parameter k_{eff} which is a weighted average of the ratio of the ionization coefficients of holes and electrons in the multiplication region and is given by:

$$F = k_{eff} * M + (1 - k_{eff})(2 - \frac{1}{M}) \qquad (14)$$

Note that the excess noise factor may sometime be expressed as:

$$F = M^x$$

where x is a constant specified by the manufacturer. In PIN diodes, where there is no gain, x is zero, and F equals one.

4.2.3 Background noise

The background power collected by the antenna can be computed by:

$$P_b = \Lambda(T,\lambda)\Omega_{rx}A_{rx}B_{opt} \quad if \quad \Omega_{rx} \le \Omega_s$$
$$\Lambda(T,\lambda)\Omega_s A_{rx}B_{opt} \quad if \quad \Omega_{rx} \ge \Omega_s$$

Where Ω_s and Ω_{rx} are the source and receiver's field of view. The moon, like the sun sustain an angle, Ω_s, of about 0.5 degree (9mrad).

The irradiance Λ is usually described by a blackbody radiation model in which given by [17]:

$$\Lambda(T,\lambda) = \frac{c^2 h}{\lambda^5}\left(\frac{1}{e^{\frac{hc}{\lambda kT}} - 1}\right) \quad \frac{W}{m^2 \mu m}$$

Where c is the speed of light, h the Planck's constant, k the Boltzman's constant and T the blackbody radiation temperature expressed in Kelvin. For example, the sun irradiance, measured outside the earth's atmosphere closely resembles that of a blackbody at 6000K. The two main background noise sources for OISL are the sun and the moon. The moon has an irradiance of $2.4*10^{-4}$ W / m^2 μm, while the sun has an irradiance of 240 W / m^2 μm [13].

4.2.4 Detector dark current noise

The detector dark current usually has two components: a surface-generated component which is unmultiplied and a much smaller bulk-generated component which undergoes multiplication.

The non-multiplicative dark current noise can be expressed as:

$$i_{nm}^2 = 2 q I_{nm} \qquad (15)$$

The multiplicative dark current noise can be written as:

$$i_m^2 = 2qM^2 F I_m \qquad (16)$$

where

q is the electronic charge
I_{nm}, I_m are the non-multiplicative and multiplicative dark current components
M the detector average gain
F the detector excess noise factor

Note that the multiplicative dark current noise is only present in detectors such as avalanche photodiodes (APDs) where the generated electrical signal undergoes multiplication to create higher current.

4.2.5 Thermal noise

The thermal noise, due to the resistive part of the detector can be expressed as:

$$i_{th}^{2} = 4 k T \qquad (17)$$

where

k is the Boltzman constant

T the effective noise temperature of the feedback resistor in °K.

4.2.6 Circuit noise

When a FET amplifier is used in the front end, following the detector, noise is introduced and may be define by [16]:

$$i_c^{2} = \left(\frac{4kT}{R_L} \left(1 + \frac{\Gamma}{g_m R_L} \right) + 2qI_{gate} \right) I_2 B + 4kT\Gamma \frac{(2\pi C_T)}{g_m} I_3 B^3 \qquad (18)$$

where

R_L is the load resistor

Γ a numerical factor given by the FET material (0.7 for Si-APD)

g_m the transconductance of the FET

I_2, I_3 , Personick's constants determined by the pulse shape and detector transfer function

C_T total load capacitance

4.2.7 Total Noise Contribution

The total noise power spectral density is the quadrature sum of all noise density contribution and is given by:

$$i_{noise}^{2} = i_{SN}^{2} + i_m^{2} + i_{nm}^{2} + i_{th}^{2} + i_c^{2} \qquad (19)$$

The signal-to-noise ratio (SNR) can be expressed in terms of the total signal power to total noise power. The SNR can thus be written as:

$$SNR = \frac{(P_{rx\_opt}\eta_d)^2}{i_{noise}^{2}} \qquad (20)$$

Table 13 gives typical values of detector parameters required in the noise analysis and Figure 14 shows the shot noise and thermal noise contributions for various photodetectors as a function of the detected optical power. Note that for the PIN diode curve, valid for an InGaAs and a SI PINs, the noise level is limited by thermal noise (constant noise level). Only above –14 dBm can the effect of shot noise be seen when the noise level starts to increase. For the APDs, the noise levels become shot noise limited around –20 dBm for the InGaAs APD and around –14 dBm for the Si APD when the relations between the noise level and the input power become linear.

Table 13 Detector parameters

Detector efficiency	η_d	0.8 A/W
Detector temperature	T	300 K
Detector gain	M	1 for PIN 50 for InGaAs APD 150 for Si_APD
Multiplicative current	I_m	10nA for InGaAs APD 1 pA for Si_APD
Non-multiplicative current	I_{nm}	10 nA
Ionization coefficient	k_{eff}	0 for PIN 0.5 for InGaAs APD 0.008 for Si_APD
Detector load capacitance	C_T	6 pF
Personick's constants	I_2 I_3	0.45 0.03

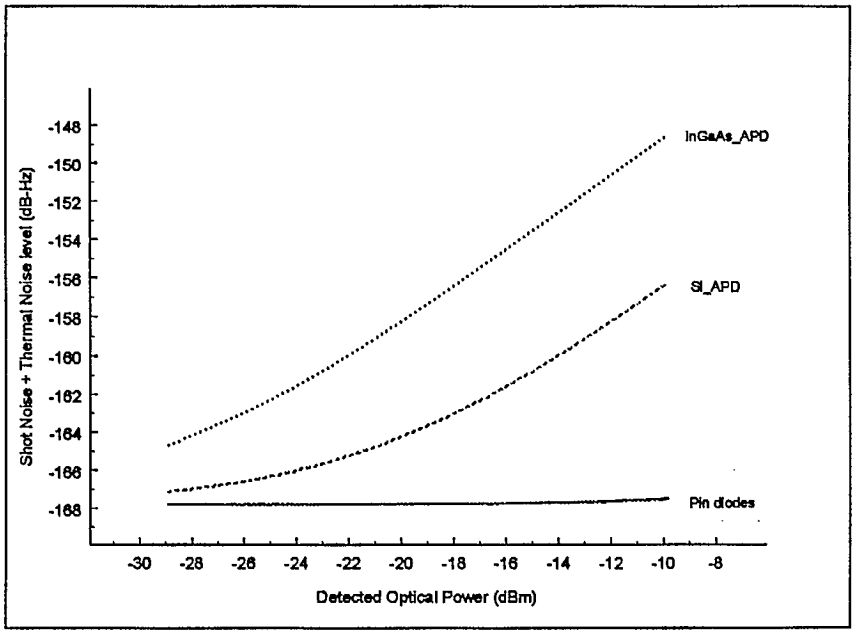

Figure 14 Shot noise plus thermal levels for various photodetector types as a function of detected power. The PIN diode curve represents both the InGaAs and the Si PINs.

4.3 Error Probability

The bit error probability depends on the signal to noise ratio and on the modulation format used. Modulation techniques can be broken down into two main categories: coherent or non-coherent. Coherent techniques rely on the phase information of the signal whereas non-coherent will depend on amplitude level or position in time. With coherent techniques, a second source, called a local oscillator, is required at the receiver to retrieve the phase information of , or demodulate the incoming signal. This is not needed for non-coherent techniques.

The main modulation formats for coherent techniques include: BPSK, QPSK and QAM. For non-coherent techniques, the most common formats are On-Off keying and pulse position modulation. In this report, only non-coherent On-Off keying (OOK) will be studied as it is the most popular form of modulation.

4.3.1 Non-coherent On-Off shift Keying (OOK)

In a non-coherent OOK, which is also called binary ASK, the laser is either on or off to represent a one or a zero. At the receiver, demodulation is done by integrating the detected signal over the bit period and comparing this value to a threshold. If the optimum threshold is used, then the probability of bit error is:

$$P_b = \frac{1}{2} erfc\left(\frac{I_s}{\sqrt{2}\ (\sigma_0 + \sigma_1)} \right) \qquad (21)$$

where:

I_s = Photo-current generated by the detected signal power

σ_0 = noise variances, when the signal is not present, due to background noise, dark current, thermal noise

$$\sigma_0^2 = i_s^2 + i_b^2 + i_d^2 + i_t^2$$

σ_0 = noise variances, when the signal is present, due to background noise, dark current, thermal noise

$$\sigma_0^2 = i_s^2 + i_b^2 + i_d^2 + i_t^2$$

From the link budget and noise analysis, one can compute the performance of an OOK link. Figure 15 gives the bit error rate curve (BER) as a function of the received power for three bit rates. The parameters given in Table 12 and Table 13 are assumed. Figure 16 shows bit error rate curves for a 2.5 Gbps transmission and various photodetectors as a function of the received power.

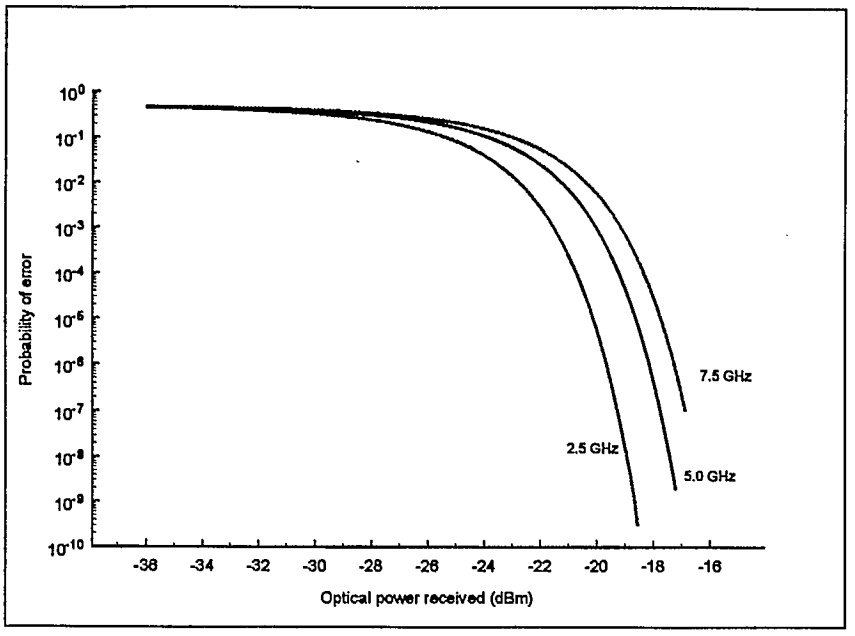

Figure 15 Bit error rate as a function of the optical power detected for various data rates using a InGaAs PIN as photodetector. No-background noise is considered.

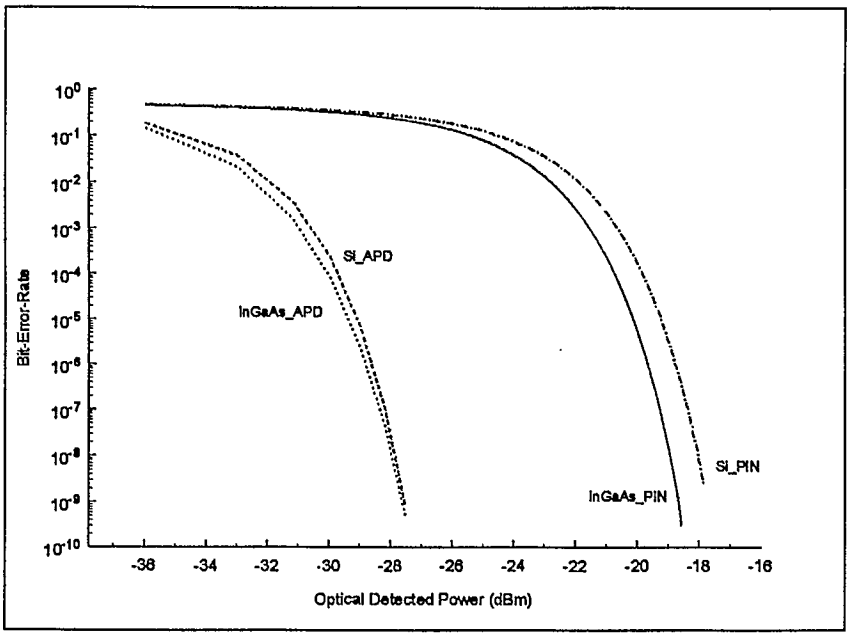

Figure 16 Bit error rate as a function of the optical power detected for various photodetectors. No-background noise is considered and a data rate of 2.5 Gbps is assumed.

5.0 CONCLUSION

The wide variety of proposed satellite systems requiring optical intersatellite links, renders the task of defining generic system specifications somewhat difficult. The orbital parameters differ widely from low-earth orbit to geostationary locations making the tracking requirements different. The data rates and link ranges are also very different from systems to system making the antenna aperture and optical power parameters different. Moreover, the proposed systems are still evolving and the orbital and link parameters are still changing. Nonetheless, a system analysis framework can be defined based on preliminary system parameters. Acquisition and tracking requirements, link budget, antenna size can be roughly evaluated.

In this report, two global communications systems are studied: Teledesic and Celestri. Orbital simulations are done to evaluate cross-link parameters such as azimuth, elevation and range. It is found that for Celestri, intersatellite links can be maintained at all time, but for Teledesic, outages periods of 3 to 6 minutes are required twice per orbit when the satellites crosses the poles. Without those outages, the telescope gimbals would have to scan over 360° in azimuth and 90° in elevation. Allowing communications when the satellites are within ±85° of longitude reduces the Teledesic telescope gimbal requirements to ±81° in azimuth and ±8° in elevation. The Celestri system has requirements somewhat similar with, ±75° in azimuth and ±7° in elevation. As for the cross-link distances, the Teledesic constellation shows ranges between 150km to 4200km, whereas for Celestri, the ranges span from 2000km to 6000km. Range, azimuth and elevation change rates have also been computed and values are given in Figures and Tables in the report.

A link budget analysis has also been done with a detailed description presented in Annex. It is shown that for a 5000km link, a 1 watt transmitter coupled with a 15 cm telescope could achieve a 10^{-9} bit-error rate when using an avalanche photodiode in the receiver. Using optical amplifiers in both the transmitter and receiver could reduce the laser power to commercially available values without significantly increasing the noise power level.

The present analysis was focused towards the elaboration of a technical base for the definition of OISL parameters. It was found that none of the system requirements are impossible to achieve with today's technology. The challenge however is to build a system which is light, compact and offer high performance. Future study could therefore be focused towards the analysis of present OISL technology and system integration and to investigate areas of possible improvements. For example, the pointing and tracking units could be investigated as well as the use of fiber optics instead of free space propagation inside the telescope.

REFERENCES

[1] Freidell James E., "Do future commercial broadband communication satellites really need laser communication inter-satellite links (ISLs)?", SPIE vol 2990, 1997.

[2] MPB Technologies "Phase 1 of a study on laser milsatcom", DSS File no. 21SU.36001-1-1976, April 1982.

[3] MPB Technologies, " The development of heterodyne-based optical intersatellite communications – Final report", DSS contract no. 1ST84-00177, June 1986.

[4] MPB Technologies "Technology development for wideband intersatellite laser communication systems", DSS contract no. 36001-7-3591/01-ST, June 1990

[5] MPB Technologies "Instruction manual for CRC laser experimental communication system" DSS contract no. 36001-3-0355, 1984

[6] Bélisle Claude, Bergevin Richard, Drouin Annie, "Rapport final Projet de communications spatiale par lase CO_2" Rapport du CRC 93-002, Communications Research Centre, March 1993.

[7] MPB Technologies "Technology for a wideband intersatellite lasercom", DSS contract no. 41ST.36001-6-3573/01-ST, February 1998.

[8] SPAR Aerospace Limited, CAL Corporation, GE Canada, "Optical intersatellite link system study" DSS contract no. 027ST-36001-0-3600, October 1991

[9] COMDEV Limited, CAL Corporation, EG&G optoelectronics Canada, SPAR Aerospace Limited National Optics Institute " Optical intersatellite link – final report", for the Canadian Space Agency Advanced SatCom program, January 1997

[10] Comdev Limited "RF intersatellite link", ", for the Canadian Space Agency Advanced SatCom program, March 1997

[11] CAL Corporation, "Optical intersatellite links (OISL)" DSS contract no. U6800-7-0917/001/ST, report pending

[12] COMDEV Limited, "Optical intersatellite link", part of a DSS contract no. U6800-7-0916/001/ST, report pending

[13] Lambert S.G. Casey W.L. "Laser Communications in Space", Artech House, 1995

[14] Klein B.J. Degnan J.J. "Optical Antenna Gain. 1: Transmitting Antenna" Applied optics, vol. 13, No.9, Sept 1974

[15] Klein B.J. Degnan J.J. "Optical Antenna Gain. 1: Receiving Antenna" Applied optics, vol. 13, No.10, Oct 1974

[16] Okoshi T. et als, "Computation of bit error rate of various heterodyne and coherent type optical communication schemes, Journal of optical communications, vol 2 no. 3 , 1981 p 89-96.

[17] Gagliardi R.M., Karp S. "Optical communications", Second Edition, Wiley series in telecommunications and signal processing, Proakis J.G. editor, 1995, ISBN 0-471-54287-3.

Appendix A

Bit Error Rate Analysis

References

1. Lambert S.G., Casey W.L. "Laser Communications in Space", Artech House, 1995, ISBN 0-89006-722-8

2. Gagliardi R.M., Karp S. "Optical communications", Second edition, Wiley series in telecommunications and signal processing, Proakis J.G. editor, 1995 ISBN 0-471-54287-3

3. Weichel H., "Atmospheric propagation of laser beams", Course Note form SPIE OE Lase 90.

4. Klein B.J. Degnan J.J. , "Optical Antenna Gain. 1: Transmitting Antenna" Applied Optics, vol.13, No 9, Sept 1974

5. SPAR Aerospace, "Optical Intersatellite Link System Study, Vol 1 Final Report", DSS contract 027ST-36001-0-3600 Oct. 1991

6. Pratt W.K., " Laser Communication Systems", Wiley & sons, 1969

7. Klein B.J. Degnan J.J. , "Optical Antenna Gain. 1: Receiving Antenna" Applied Optics, vol.13, No 10, Oct.1974

8. Ross M. "Laser Receivers Devices, Techniques, Systems" Wiley, 1996

9. Karp S., Gagliardi R., Moran S., Stotts L., "Optical Channels fibers, clouds, water, and the atmosphere", Plenum Press, 1988,

Units Definitions

$\mu m := 10^{-6} \cdot m$	$A := amp$	$W := watt$	$C := coul$	$s := sec$
$nm := 10^{-9} \cdot m$	$nA := 10^{-9} \cdot A$	$mW := 10^{-3} \cdot W$	$J := joule$	$\mu rad := 10^{-6} \cdot rad$
	$pA := 10^{-12} \cdot A$	$\mu W := 10^{-6} \cdot W$	$\Omega := ohm$	
		$nW := 10^{-9} \cdot W$		

Parameters Definition

Global Constants

Speed of light in free space $c := 3 \cdot 10^{8} \cdot \frac{m}{s}$

Planck Constant $h := 6.625 \cdot 10^{-34} \cdot J \cdot s$

Electron Charge $q := 1.602 \cdot 10^{-19} \cdot C$

Boltzman Constant $k := 1.38 \cdot 10^{-23} \cdot \frac{J}{K}$

Decibel

$dB := 1$

$dBm := 1$

Detector_types

$InGaAs\_PIN := 0$

$InGaAs\_APD := 1$

$Si\_PIN := 2$

$Si\_APD := 3$

Background Noise Sources

$NO\_BACKGROUND := 0$

$BLACKBODY := 1$

$MOON := 2$

$SUN := 3$

Number of detector type $det\_type\_num := 3$

Near_field_types

$UNIFORM := 0$

$GAUSS\_ON\_AXIS := 1$

$GAUSS\_OFF\_AXIS := 2$

Counters

Transmitter power levels P_L

$imax := 80$

$i := 0 .. imax$ $\quad P_{L_i} := (1 + i) \cdot 1 \cdot W$

Data bandwidth B_{RF}

$jmax := 2$

$j := 0 .. jmax$ $\quad B_{RF_j} := (1 + j) \cdot 2.5 \cdot GHz$

Pointing angle error ψ_{pt}

$nmax := 5$

$n := 0 .. nmax$ $\quad \psi_{tx\_pt_n} := (1 + n) \cdot 1 \cdot \mu rad$

Antenna size $D_{ant} = D_{tx\_aper} = D_{rx\_aper}$

$pmax := 4$

$p := 0 .. pmax$ $\quad D_{ant_p} := (1 + p) \cdot 5 \cdot cm$

Range R_r

$rmax := 14$

$r := 0 .. rmax$ $\quad R_r := (1 + r) \cdot 500 \cdot km$

TRANSMITTER CONSTANTS

Laser wavelength

$\lambda := 1550 \cdot nm$

Laser Frequency

$\nu := \frac{c}{\lambda}$ $\quad \nu = 1.935 \cdot 10^{14} \cdot Hz$

Laser Power

$P_{L\_dB_i} := 10 \cdot \log\left(\frac{P_{L_i}}{1 \cdot mW}\right)$

P_L defined in globalconstant section

Optical Amplifier Gain

$G_{tx\_opt\_amp\_dB} := 0$ $\quad G_{tx\_opt\_amp} := 10^{\frac{G_{tx\_opt\_amp\_dB}}{10}}$

Antenna aperture diameter

$D_{tx\_aper_p} := D_{ant_p}$

Transmitter obscuration diameter secondary mirror and support structure

$D_{tx\_obs_p} := 0.2 \cdot D_{tx\_aper_p}$

Note: Typical value for D_{tx_obs} / D_{tx_aper} for a Cassegrain style telescope is around 0.2

Transmitter diverging angle

For an unobscured beam. $\theta_{tx\_div_p} := \frac{\lambda}{D_{tx\_aper_p}}$

Ref: [8] p.7
Ref [9] p. 4

Example: for $D_{tx\_aper_0} = 5 \cdot cm$ $\quad \theta_{tx\_div_0} = 31 \cdot \mu rad$

Note: For a centrally obscured aperture, the beam divergence decreases slightly with increasing obscuration. Fig. 10 in ref 4, shows the degradation of the half angle cone for increased obscuration

Transmitter field of view

For an unobscured beam: $\Omega_{t_p} := \frac{4 \cdot \lambda^2}{\pi \cdot \left(D_{tx\_aper_p}\right)^2}$

Ref [9] p. 8
Ref: [8] p. 7

Transmitter beam waist radius measured at the $1/e^2$ intensity point

$\omega_0 := \frac{D_{tx\_aper}}{3}$

This ensures that 99% of a Gaussian beam will be propagated [ref 3 p.17]

Example: $\omega_{0_0} = 0.017 \cdot m$

Transmitter telescope gain

Ref 1 p.97-99

The classical telescope gain formula is written for an ideal, uniformly illuminated circular aperture of diameter D_{tx} and the gain, at an angle θ, is given by:

$$G(\theta) = \left[\frac{\pi D_{tx}}{\lambda}\right]^2 * \left[\frac{2J_1(\pi \sin(\theta)) D_{tx} / \lambda}{\pi \sin(\theta) D_{tx} / \lambda}\right]^2$$

which, on axis is simplified to:

$$G(0) = \left[\frac{\pi D_{tx}}{\lambda}\right]^2$$

However, in laser comm systems, the near-field profile is Gaussian or nearly-Gaussian, with an amplitude plane wave with a waist size, ω_0 (the radius of the point in the beam where the intensity drops to $1/e^2$, and wavelength λ, impinging onto a circular aperture D_{tx_aper} with an obscuration D_{tx_obs}.

$$G(\theta, \alpha) = \left[\frac{\pi D_{tx}}{\lambda}\right]^2 * \left[2\alpha^2 \left[\int_0^1 e^{-\alpha^2 u} J_0\left(\frac{\pi D_{tx}}{\lambda} \sin(\theta)\sqrt{u}\right)\right] du\right]^2$$

with $\alpha = D_{tx} / 2w_0$ where w_0 is the beam waist radius

Here we can distinguish if the far field is on-axis or off-axis. With on-axis gain, θ=0, and $J_0(0)$ =1, which simplifies the equation. With off-axis gain, if we consider only the gain down to the $1/e^2$ level, the equation can also be approximated by a Gaussian profile out to this level. Here, the gain is calculated to the pointing error ψ_{tx_pt}

Defining:

$$\alpha_p := \frac{D_{tx\_aper_p}}{2 \cdot \omega_{0_p}} \qquad \gamma_p := \frac{D_{tx\_obs_p}}{D_{tx\_aper_p}} \qquad X(\theta_{off\_axis}, p) := \frac{2 \cdot \pi}{\lambda} \cdot D_{tx\_aper_p} \cdot \sin(\theta_{off\_axis})$$

We obtain the far field telescope gain [ref 4]:

$$G_{tx}(\theta_{off\_axis}, p) := \left(\frac{\pi \cdot D_{tx\_aper_p}}{\lambda}\right)^2 \cdot 2 \cdot (\alpha_p)^2 \cdot \left[\int_{(\gamma_p)^2}^1 \exp\left[-(\alpha_p)^2 \cdot u\right] \cdot J0\left(X(\theta_{off\_axis}, p) \cdot \sqrt{u}\right) du\right]^2$$

Note: If the near-field beam is Gaussian, and there is no misalignment, i.e. on-axis and $\theta_{off\text{-}axis}=0$, than the antenna gain equation reduces to:

$$G_{tx}(p) := \left[\left(\frac{\pi \cdot D_{tx\_aper_p}}{\lambda}\right)^2 \cdot \left[\frac{2}{(\alpha_p)^2} \cdot \left[e^{-(\alpha_p)^2} - e^{-(\gamma_p)^2 \cdot (\alpha_p)^2}\right]^2\right]\right]_{\blacksquare}$$

Note: If the near-field beam is uniform, and there is no misalignment, i.e. on-axis and $\theta_{off\text{-}axis}=0$, than the antenna gain equation reduces to:

$$G_{tx}(p) := \left[\frac{\pi \cdot \left(D_{tx\_aper_p}\right)}{\lambda}\right]^2 \cdot \left[1 - (\gamma_p)^2\right]_{\blacksquare}$$

Note: The central obscuration creates a need to optimize the trade-off between α and γ in an effort to maximize the net power being passed through the annular aperture. Although the relationship is a complicated function, Klein and Degnan [ref 4] show how to derive the following approximation exact at $\gamma=0$ and accurate to within +/- 1% for $\gamma<0.4$.

$$\alpha_{optimum_p} := 1.12 - 1.3 \cdot (\gamma_p)^2 + 2.12 \cdot (\gamma_p)^4$$

Note: Gaussian beam profile and central obscuration loss (dB):

$$L_{Gauss\_dB_p} := 10 \cdot \log\left[\frac{2}{(\alpha_p)^2} \cdot \left[e^{-(\alpha_p)^2} - e^{-(\gamma_p)^2 \cdot (\alpha_p)^2}\right]^2\right]$$

Example: assume $D_{tx\_aper_0} = 5 \cdot cm$, $D_{tx\_obs_0} = 1 \cdot cm$ Then $L_{Gauss\_dB_0} = -2.358 \cdot dB$

Note: Pointing Error Loss (dB)

$$L_{pt}(\psi_{tx\_pt}, p) := 10 \cdot \log\left[\frac{2 \cdot (\alpha_p)^2 \cdot \left[\int_{(\gamma_p)^2}^{1} \exp\left[-(\alpha_p)^2 \cdot u\right] \cdot J0\left(X(\psi_{tx\_pt}, p) \cdot \sqrt{u}\right) du\right]^2}{\left[\frac{2}{(\alpha_p)^2} \cdot \left[e^{-(\alpha_p)^2} - e^{-(\gamma_p)^2 \cdot (\alpha_p)^2}\right]^2\right]}\right]$$

Example: assume $D_{tx\_aper_0} = 5 \cdot cm$

$D_{tx\_obs_0} = 1 \cdot cm$

$Pointing\_error := 2 \cdot \mu rad$

Then $L_{pt}(2 \cdot \mu rad, 0) = -0.128 \cdot dB$

Transmitter antenna field of view [ref 2 p.8]:

$$\Omega_{tx}(p) := \frac{4 \cdot \pi}{G_{tx}(0, p)}$$ in steradians

Example: Assume $D_{tx\_aper_0} = 5 \cdot cm$

then $\Omega_{tx}(0) = 2.106 \cdot 10^{-9}$

Wavefront Loss

The ability The wavefront loss is associated with aberrations of the optical signal by the optical elements in the transmit path. An rms quantification of these error contribution is typically used to determine the loss due to wavefront error and is expressed as $\sigma = \lambda/x$ where x is in the order of 10 for most laser communications systems.

When a number of optical surfaces are involved, the net overall σ_{rms} can be determined by:

$$\sigma_{rms} = \sqrt{\sigma_1^2 + \sigma_2^2 + \ldots + \sigma_n^2}$$

Assuming that the overall rms wavefront error is: $\sigma_{rms} := \frac{\lambda}{10}$

The wavefront error loss can be computed using:

$$L_{tx\_wf} := e^{-\left(\frac{2 \cdot \pi \cdot \sigma_{rms}}{\lambda}\right)^2}$$

$L_{tx\_wf} = 0.674$

$L_{tx\_wf\_dB} := 10 \cdot \log(L_{tx\_wf})$

Note: Typical values for optical elements quality:

Flat mirrors and plates (<4")	λ/200
Flat mirrors and plates (4"-14")	λ/50
Spherical mirrors (<14")	λ/40
Spherical lenses (<14")	λ/40
Cube beamsplitters	λ/20

Ref 5: p.3-72

Transmissivity Loss:

Transmission loss is caused by the optical lenses and coating in the optical network which have finite transmissivity at the desired wavelength. For a typical ISL system concept containing

1 thermal window	1-2 fine pointing mirrors
1 primary mirror	3-4 beamsplitters
1 secondary mirror	3-4 lenses at the laser (or detector)
~ 10 lenses in the eye piece	

the transmissivity would be on the order of 80%

Transmissivity of various optical elements at 800 nm:

Bulk fused silica:	0.999 per 25 mm
Bulk SF6 G5	0.964 per 25 mm
Bulk SK4 G13	0.991 per 25 mm

For this analysis, we will assume:

$$L_{tx\_opt} := 0.8 \qquad L_{tx\_opt\_dB} := 10 \cdot \log\left(L_{tx\_opt}\right)$$

$$L_{tx\_opt\_dB} = -0.969$$

LINK

Propagation Loss $L_{R_r} := \left(\frac{\lambda}{4 \cdot \pi \cdot R_r}\right)^2$ $L_{R\_dB_r} := 10 \cdot \log\left(L_{R_r}\right)$

Background Radiation:

Ref 2 p.59-68
Ref 6 p 111-127
The background sources are divided into two basic types: a) the extended background, assumed to occupy the entire background, and therefore is present in any receiver field of view, and b) discrete or point sources that are more localized but also more intense and may or may not be in the receiver field of view. Examples of extended background sources are the clouds, snow and ice and the starfield. Examples of point sources are the stars, the planets, the moon, the sun.

Extended point sources are most often described by their spectral radiance function $W_b(\lambda)$, defined as the power radiated at wavelength λ per cycle of bandwidth into a unit solid angle per unit of source area. If the radiation source has an area of A_s, then the total power collected depends on the portion of the source lying within the receiver field of view, Ω_{rx}, Thus the background power collected at the receiver in a wavelength bandwidth, B_{opt}, around a wavelength λ is given by:

$$P_b = W_b(\lambda)\, \Omega_{rx}\, A_{rx}\, B_{opt} \quad \text{if } \Omega_{rx} < \Omega_s \qquad \text{ref: [2] p.60}$$
$$W_b(\lambda)\, \Omega_s\, A_{rx}\, B_{opt} \quad \text{if } \Omega_s < \Omega_{rx}$$

where Ω_s is the source field of view and is equal to A_s/Z^2 where A_s is the source area and Z its distance

For localized point sources, which emits equally in all directions (Lambertian source), producing noise fields for which $\Omega_s < \Omega_{rx}$, it is convenient to define the source irradiance at wavelength λ as the product of

$$N_b(\lambda) = W_b(\lambda)\, \Omega_s$$

and therefore the background power collected can be computed by:

$$P_b = N_b(\lambda)\, A_{rx}\, B_{opt}$$

Note: most background sources are described by a blackbody radiation model in which the radiance is given by:

$$W_{blackbody}(T,\lambda) := \frac{c^2 \cdot h}{\lambda^5} \cdot \left(\frac{1}{e^{\frac{h \cdot c}{\lambda \cdot k \cdot T}} - 1} \right) \qquad \frac{W}{(m^2\ \mu m)} \qquad \text{ref: [2] p.61}$$

where T is the temperature of the radiation in degrees Kelvin, c the speed of light, h is Planck's constant and k the Boltzman constant. For example, the sun irradiance, measured outside the Earth's atmosphere closely resembles a blackbody at 6000K.

Background irradiance energy density measured, at 1550 nm, for various sources, [Ref 1 p.155]

$$W_b(background\_source) := \begin{cases} 2.4 \cdot 10^{-4} \cdot \frac{W}{m^2 \cdot \mu m} & \text{if background\_source=MOON} \\ \left(204 \cdot \frac{W}{m^2 \cdot \mu m} \right) & \text{if background\_source=SUN} \\ \left(0 \cdot \frac{W}{m^2 \cdot \mu m} \right) & \text{if background\_source=NO\_BACKGROUND} \end{cases}$$

Note: The moon, like the sun sustends an angle of about 0.5degree (9mrad)

RECEIVER

Since the receiver telescope is most often the same as the transmitter telescope, the same values will be assumed

Receiver aperture diameter $D_{rx\_aper} := D_{ant}$

Receiver obscuration diameter $D_{rx\_obs} := D_{tx\_obs}$

Note: Typical value for D_{rx_obs} / D_{rx_aper} for a Cassegrain style telescope is around 0.2

Effective Receiver Aperture Area

$$A_{rx_p} := \frac{\pi \cdot \left(D_{rx\_aper_p}\right)^2}{4} \cdot \left[1 - \left(\frac{D_{rx\_obs_p}}{D_{rx\_aper_p}}\right)^2\right]$$

Antenna F number $F_{ant} := 5$

Receiver telescope gain

At the receiver, the incoming beam can be considered to be uniformly distributed. The gain equation then correspond to the usual equation $4\pi A/\lambda^2$. If we include the effect of obstructions from the central mirror and support ($1-\gamma^2$) and various losses at the detector such as fractional signal power detected, the telescope gain can be written as [ref 7

Defining: $$\gamma_{rx_p} := \frac{D_{rx\_obs_p}}{D_{rx\_aper_p}}$$

$$\zeta_{det}\left(D_{det}, p\right) := \frac{2}{\left[1 - \left(\gamma_{rx_p}\right)^2\right]} \cdot \int_0^{\frac{2\cdot\pi}{\lambda} \cdot \frac{D_{det}}{4 \cdot F_{ant}}} \frac{\left(J1(u) - \gamma_{rx_p} \cdot J1\left(\gamma_{rx_p} \cdot u\right)\right)^2}{u} du$$

where D_{det} is the diameter of the detector

$$G_{rx}\left(D_{det}, p\right) := \left(\frac{\pi \cdot D_{rx\_aper_p}}{\lambda}\right)^2 \cdot \left[1 - \left(\gamma_{rx_p}\right)^2\right] \cdot \zeta_{det}\left(D_{det}, p\right)$$

Receiver Pointing Loss $L_{rx\_pt\_dB} := -0.5$ $L_{rx\_pt} := 10^{\frac{L_{rx\_pt\_dB}}{10}}$ $L_{rx\_pt} = 0.891$

Receiver field of view
Ref.2 p.45 & 47 $\Omega_{rx\_fov}(D_{det}, p) := \frac{4 \cdot \pi}{G_{rx}(D_{det}, p)}$ steradian

Example: $\Omega_{rx\_fov}(100 \cdot \mu m, 1) = 3.321 \cdot 10^{-10}$

If the receiver antenna is diffraction limited, the spot size, as defined by the Airy disk is given by:

$$d_D = \frac{2.44F\lambda}{d_R}$$

where F is the lens focal length, d_D is the diameter of the focused incident beam, d_R is the receiver antenna diameter and λ the optical wavelength.

The receiver field of view θ_R is given by:

$$\theta_R = \frac{d_P - d_D}{F}$$

where d_P is the photodetector diameter

Receiver optics transmissivity loss $L_{rx\_opt} := L_{tx\_opt}$ $L_{rx\_opt\_dB} := 10 \cdot \log(L_{rx\_opt})$

Receiver Optical Amplifier gain $G_{rx\_opt\_amp\_dB} := 0$ $G_{rx\_opt\_amp} := 10^{\frac{G_{rx\_opt\_amp\_dB}}{10}}$

Receiver Optical Amplifier Noise Figure $NF_{optamp} := 5$ Not used as of 19 feb

Optical bandpass filter $B_{opt} := 10 \cdot nm$

DETECTOR

Detector diameter $D_{det} := 100 \cdot \mu m$

Detector efficiency Ref.1 p.244

$$\eta_d(\text{detector\_type}) := \begin{cases} \left(0.8 \cdot \frac{A}{W}\right) & \text{if detector\_type=InGaAs\_PIN} \\ \left(0.8 \cdot \frac{A}{W}\right) & \text{if detector\_type=InGaAs\_APD} \\ \left(0.65 \cdot \frac{A}{W}\right) & \text{if detector\_type=Si\_PIN} \\ \left(0.65 \cdot \frac{A}{W}\right) & \text{if detector\_type=Si\_APD} \end{cases}$$

Detector Temperature $T_d := 300 \cdot K$

Detector Gain Ref.1 p.244

$$G_{det}(\text{detector\_type}) := \begin{cases} 1 & \text{if detector\_type=InGaAs\_PIN} \\ 10 & \text{if detector\_type=InGaAs\_APD} \\ 1 & \text{if detector\_type=Si\_PIN} \\ 10 & \text{if detector\_type=Si\_APD} \end{cases}$$

Multiplicative dark current Ref.1 p.244

$$I_m(\text{detector\_type}) := \begin{cases} 0 \cdot nA & \text{if detector\_type=InGaAs\_PIN} \\ 10 \cdot nA & \text{if detector\_type=InGaAs\_APD} \\ 1 \cdot pA & \text{if detector\_type=Si\_PIN} \\ 1 \cdot pA & \text{if detector\_type=Si\_APD} \end{cases}$$

Non Multiplicative Dark Current Ref.1 p.244

$$I_{nm}(\text{detector\_type}) := \begin{cases} 10 \cdot nA & \text{if detector\_type=InGaAs\_PIN} \\ 10 \cdot nA & \text{if detector\_type=InGaAs\_APD} \\ 10 \cdot nA & \text{if detector\_type=Si\_PIN} \\ 10 \cdot nA & \text{if detector\_type=Si\_APD} \end{cases}$$

Ionization coefficient Ref.1 p.244

$$k_{eff}(det\_type) := \begin{cases} 0 & \text{if } det\_type = InGaAs\_PIN \\ 0.5 & \text{if } det\_type = InGaAs\_APD \\ 0 & \text{if } det\_type = Si\_PIN \\ 0.008 & \text{if } det\_type = Si\_APD \end{cases}$$

Excess Noise Factor Ref.1 p.147

$$F(det\_type) := \begin{cases} 1 & \text{if } det\_type = InGaAs\_PIN \\ 1 & \text{if } det\_type = Si\_PIN \\ \left[\left[G_{det}(det\_type)\cdot k_{eff}(det\_type) + \left(1 - k_{eff}(det\_type)\right)\right]\cdot\left(2 - \frac{1}{G_{det}(det\_type)}\right)\right] & \text{otherwise} \end{cases}$$

EXAMPLE:, Consider an Si_APD with gain of $G_{det}(Si\_APD) = 10$ $F(Si\_APD) = 2.037$

For an InGaAs_APD with gain of $G_{det}(InGaAs\_APD) = 10$ $F(InGaAs\_APD) = 10.45$

Note: The InGaAs_APD will create a higher noise level than the Si_APD. The signal to noise ratio will then be lower.

Note: Others will express the excess noise factor as x where x is usually less than 1. The excess noise factor is used in the noise current density calculation along with the detector gain. The detector increases the output power by a factor of G^2*F or by G^{2+x}. The relation between F and x is then x = log(F) / log(G). In the above example x would be 0.294.

Detector Circuit Resistance $R_d := 50\cdot\Omega$

Receiver Field of view is diffraction limited

RECEIVED OPTICAL POWERS

A) SIGNAL

The received optical signal level P_{rx} is calculated from the aggregate of all gains and losses in the systems

$$P_{opt\_rx}(i,n,p,r) := P_{L_i} \cdot G_{tx\_opt\_amp} \cdot \left(G_{tx}\left(\psi_{tx\_pt_n}, p\right) \cdot L_{tx\_wf} L_{tx\_opt}\right) \cdot L_{R_r} \cdot G_{rx}\left(D_{det}, p\right) \cdot \left(L_{rx\_pt} \cdot L_{rx\_opt} \cdot G_{rx\_opt\_amp}\right)$$

$$P_{opt\_rx\_dB}(i,n,p,r) := 10 \cdot \log\left(\frac{P_{opt\_rx}(i,n,p,r)}{1 \cdot mW}\right)$$

Example,

Using		we obtain
$P_{L_{24}} = 2.5 \cdot 10^4 \cdot mW$	$D_{tx\_aper_1} = 10 \cdot cm$	$P_{opt\_rx}(24,0,1,3) = 32.049 \cdot \mu W$
$\psi_{tx\_pt_0} = 1 \cdot \mu rad$	$R_3 = 2 \cdot 10^3 \cdot km$	$P_{opt\_rx\_dB}(24,0,1,3) = -14.942 \cdot dB$

where

P_L	laser power	G_{opt}	optical amplifier gain
G_{tx} , G_{rx}	telescope gain	L_{tx_wf}	loss due to wavefront error
L_r	range loss	L_{rx_pt}	loss to mispointing
L_{tx_opt} L_{rx_opt}	loss due to optical elements transmissivity		

B) BACKGROUND

The collected background power is expressed as [ref 6 p.118]:

1. If the entire source is falling within the receiver field of view:

$$P_b(p, background\_source) := d_s^2 \cdot \Omega_{rx\_fov}\left(D_{det}, p\right) \cdot L_{rx\_opt} \cdot W_b(background\_source) \cdot \Omega_{source} \cdot B_{opt}$$

with d_s being the diameter of the source

2. If the solid angle subtended by the source at the receiver is greater than the solid angle of the receiver, (which is most of the time with optical systems)

$$P_b(p, background\_source) := \Omega_{rx\_fov}\left(D_{det}, p\right) \cdot A_{rx_p} \cdot W_b(background\_source) \cdot L_{rx\_opt} \cdot B_{opt}$$

LINK BUDGET

Assuming:

Pointing error of:	$i_{pt} := 0$	$\psi_{tx\_pt_{i_{pt}}} = 1 \cdot \mu rad$
Antenna diameter	$i_{Dant} := 1$	$D_{ant_{i_{Dant}}} = 10 \cdot cm$
Range	$i_{range} := 3$	$R_{i_{range}} = 2 \cdot 10^3 \cdot km$
Fix laser power	$i_{tx\_pow} := 29$	$P_{L_{i_{tx\_pow}}} = 3 \cdot 10^4 \cdot mW$
Counter on laser power	$i_L := 0 .. imax$	
Fix Data rates	$i_{RF} := 0$	$B_{RF_{i_{RF}}} = 2.5 \cdot GHz$
Counter on data rates	$i_{BRF} := 0 .. jmax$	

Wavelength of transmission (nm)	$\lambda = 1.55 \cdot 10^3 \cdot nm$
Transmit source average power (mW)	$P_{L_{i_{tx\_pow}}} = 3 \cdot 10^4 \cdot mW$
Optical amplifier gain (dB)	$G_{tx\_opt\_amp\_dB} = 0$
Transmit optics transmissivity Loss (dB)	$L_{tx\_opt\_dB} = -0.969$
Diameter of transmit Optics (cm)	$D_{tx\_aper_{i_{Dant}}} = 10 \cdot cm$
Transmit objective gain (dB)	$10 \cdot \log\left[\left(\pi \cdot \frac{D_{tx\_aper_{i_{Dant}}}}{\lambda}\right)^2\right] = 106.136 \cdot dB$
Diameter of central obscuration	$D_{tx\_obs_{i_{Dant}}} = 2 \cdot cm$
Transmit Gaussian beam profile and central obscuration loss (dB)	$L_{Gauss\_dB_{i_{Dant}}} = -2.358$
Wavefront error Loss (dB)	$L_{tx\_wf\_dB} = -1.715 \cdot dB$
Secondary mirror and strut blockage loss (dB)	

Pointing error (μrad)	$\psi_{tx\_pt_{i\,pt}} = 1 \cdot \mu rad$
Pointing accuracy loss (dB)	$L_{pt}\left(\psi_{tx\_pt_{i\,pt}}, i_{Dant}\right) = -0.128 \cdot dB$
Diffraction limited Tx beam angle (approx) (μrad)	$\theta_{tx\_div_{i\,Dant}} = 15.5 \cdot \mu rad$
Intersatellite link range (km)	$R_{i\,range} = 2 \cdot 10^3 \cdot km$
Range Loss (dB)	$L_{R\_dB_{i\,range}} = -264.198 \cdot dB$
Planar beam diameter at receiver (m)	$\theta_{tx\_div_{i\,Dant}} \cdot R_{i\,range} = 31 \cdot m$
Diameter of receive optics (cm)	$D_{rx\_aper_{i\,Dant}} = 10 \cdot cm$
Diameter of central obscuration	$D_{rx\_obs_{i\,Dant}} = 2 \cdot cm$
Receive objective gain (dB)	$10 \cdot \log\left[\left(\frac{\pi \cdot D_{rx\_aper_{i\,Dant}}}{\lambda}\right)^2\right] = 106.136 \cdot dB$
Central obscuration loss (dB)	$10 \cdot \log\left[1 - \left(\gamma_{i\,Dant}\right)^2\right] = -0.177 \cdot dB$
Fractional power detection loss (dB)	$10 \cdot \log\left(\zeta_{det}\left(D_{det}, i_{Dant}\right)\right) = -0.18 \cdot dB$
Secondary mirror and strut blockage loss (factor) (dB)	
Receive optical transmissivity loss (dB)	$L_{rx\_opt\_dB} = -0.969 \cdot dB$
Pointing error loss (dB)	$L_{rx\_pt\_dB} = -0.5 \cdot dB$
Optical power at detector (μW)	$P_{opt\_rx}\left(i_{tx\_pow}, i_{pt}, i_{Dant}, i_{range}\right) = 38.459 \cdot \mu W$
(dBm)	$P_{opt\_rx\_dB}\left(i_{tx\_pow}, i_{pt}, i_{Dant}, i_{range}\right) = -14.15 \cdot dBm$
LINK LOSS (dB)	$10 \cdot \log\left(\frac{P_{L_{i\,tx\_pow}}}{1 \cdot mW}\right) - P_{opt\_rx\_dB}\left(i_{tx\_pow}, i_{pt}, i_{Dant}, i_{range}\right) = 58.921 \cdot dB$

PHOTO-CURRENTS

The photo-current, i, generated by an optical signal of power P_{opt} is given by:

$$i_s := \frac{q}{h \cdot \nu} \cdot \xi \cdot P_{opt}$$ where $q\xi/h\nu$ is the detector responsivity, η_d, in A/W

$$i_s(P_{opt}, detector\_type) := \eta_d(detector\_type) \cdot P_{opt}$$

The instantaneous receiver output signal voltage v_p, is then equal to:

$$v_s := G_{det} \cdot i_s \cdot R_L$$ where G_{det} is the detector current gain and R_L the equivalent detector load

The average signal power at the receiver output is defined to be the time average of v_p^2 over a time period reciprocal to the output filter bandwidth B_{rf}. Thus for an unmodulated carrier, the signal power is:

$$S := \frac{v_s^2}{R_L} \quad \text{or} \quad S := (G_{det} \cdot i_s)^2 \cdot R_L$$

$$S := \left(G_{det} \cdot \frac{q \cdot \xi}{h \cdot \nu} \cdot P_{opt}\right)^2 \cdot R_L$$

For the optical signal

$$S_{rf}(i,n,p,r,Detec\_type) := \left(G_{det}(Detec\_type) \cdot \eta_d(Detec\_type) \cdot P_{opt\_rx}(i,n,p,r)\right)^2 \cdot R_d$$

$$S_{rf\_dBm}(i,n,p,r,Detec\_type) := 10 \cdot \log\left(\frac{S_{rf}(i,n,p,r,Detec\_type)}{1 \cdot mW}\right)$$

Example:

using:

$P_{L_{i\,tx\_pow}} = 3 \cdot 10^4 \cdot mW$ $\quad$ $\psi_{tx\_pt_{i\,pt}} = 1 \cdot \mu rad$

$D_{ant_{i\,Dant}} = 10 \cdot cm$ $\quad$ $R_{i\,range} = 2 \cdot 10^3 \cdot km$

we obtain $P_{opt\_rx\_dB}(i_{tx\_pow}, i_{pt}, i_{Dant}, i_{range}) = -14.15 \cdot dBm$ of optical signal

$S_{rf}(i_{tx\_pow}, i_{pt}, i_{Dant}, i_{range}, Si\_PIN) = 31.246 \cdot nW$ of electrical signal

$S_{rf\_dBm}(i_{tx\_pow}, i_{pt}, i_{Dant}, i_{range}, Si\_PIN) = -45.052 \cdot dBm$

$$j_{det} := 0 .. det\_type\_num$$

$$Z_{PO_r} := P_{opt\_rx\_dB}\left(i_{tx\_pow}, i_{pt}, i_{Dant}, r\right) \qquad Z_{Pelec_{r,j_{det}}} := S_{rf\_dBm}\left(i_{tx\_pow}, i_{pt}, i_{Dant}, r, j_{det}\right)$$

Electrical power generated versus Optical power detected

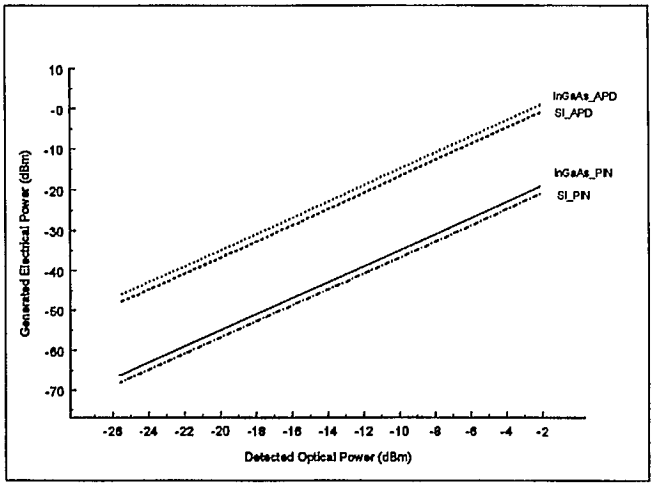

NOISE CURRENT DENSITY

The photo-detection can be considered as a Poisson process and therefore the shot noise can be expressed as [Ref 6, p.156]

A) Signal Shot Noise

$$N_{s\_sn}(i,n,p,r,Detec\_type) := 2 \cdot q \cdot i_s\left(P_{opt\_rx}(i,n,p,r), Detec\_type\right) \cdot G_{det}(Detec\_type)^2 \cdot F(Detec\_type)$$

Example: $$10 \cdot \log\left(\frac{N_{s\_sn}\left(i_{tx\_pow}, i_{pt}, i_{Dant}, i_{range}, InGaAs\_PIN\right) \cdot R_d \cdot Hz}{W}\right) = -2.131 \cdot 10^2 \cdot dB$$

B) Background noise

$$N_{b\_sn}(p,Detec\_type,Back\_src) := 2 \cdot q \cdot i_s\left(P_b(p,Back\_src), Detec\_type\right) \cdot G_{det}(Detec\_type)^2 \cdot F(Detec\_type)$$

$$\left[N_{b\_sn}\left(i_{Dant}, InGaAs\_APD, NO\_BACKGROUND\right) \cdot \left(R_d \cdot Hz\right)\right] = 0 \cdot W$$

C) Detector Dark Noise

Multiplicative Dark current

$$N_m(Detec\_type) := 2 \cdot q \cdot G_{det}(Detec\_type)^2 \cdot F(Detec\_type) \cdot I_m(Detec\_type)$$

$$10 \cdot \log\left[\frac{N_m(InGaAs\_APD) \cdot \left(R_d \cdot Hz\right)}{W}\right] = -217.762 \cdot dB$$

Non multiplicative dark current

$$N_{nm}(Detec\_type) := 2 \cdot q \cdot I_{nm}(Detec\_type)$$

$$10 \cdot \log\left(\frac{N_{nm}(InGaAs\_APD) \cdot R_d \cdot Hz}{W}\right) = -247.953 \cdot dB$$

D) Thermal

$$N_t := \frac{4 \cdot k \cdot T_d}{R_d} \qquad 10 \cdot \log\left(\frac{N_t \cdot R_d \cdot Hz}{W}\right) = -197.809 \cdot dB$$

E) Circuit Noise

NOTE: Other things will increase the noise level: Optical and microwave amplifiers have noise figures. e.g. EDFA has a NF of about 4 dB.

Total Noise Contribution:

$i_{pow} := 0 .. imax$

Received Power $\quad Z2_{i_{pow}} := P_{opt\_rx\_dB}\left(i_{pow}, i_{pt}, i_{Dant}, i_{range}\right)$

Shot noise $\quad N_{sn_{i_{pow}}} := 10 \cdot \log\left(\frac{N_{s\_sn}\left(i_{pow}, i_{pt}, i_{Dant}, i_{range}, Si\_APD\right) \cdot R_d \cdot Hz}{mW}\right)$

Thermal noise $\quad N_{therm} := 10 \cdot \log\left(\frac{N_t \cdot R_d \cdot Hz}{mW}\right) \qquad N_{therm} = -167.809 \cdot dBm$

Total noise $\quad N_{total_{i_{pow}}} := 10 \cdot \log\left[\frac{\left(N_{s\_sn}\left(i_{pow}, i_{pt}, i_{Dant}, i_{range}, Si\_APD\right) + N_t\right) \cdot R_d \cdot Hz}{mW}\right]$

Using a Si APD, the system becomes shot noise limited for received power levels above -10 dBm

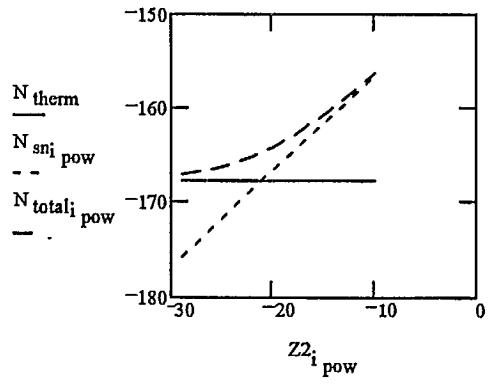

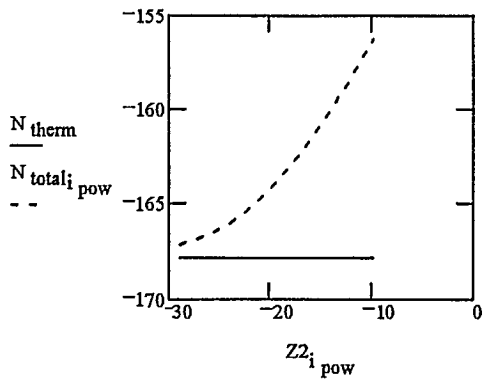

$$j_{det} := 0 .. det\_type\_num$$

$$N_{tot\_dB_{i_{pow}, j_{det}}} := 10 \cdot \log\left[\frac{\left(N_{s\_sn}\left(i_{pow}, i_{pt}, i_{Dant}, i_{range}, j_{det}\right) + N_t\right) \cdot R_d \cdot Hz}{mW}\right]$$

Total Noise contribution versus Received optical signal power.

Note: For PIN diodes, the system is thermal noise limited. For APDs, the system starts thermal noise limited but rapidly goes shot noise limited

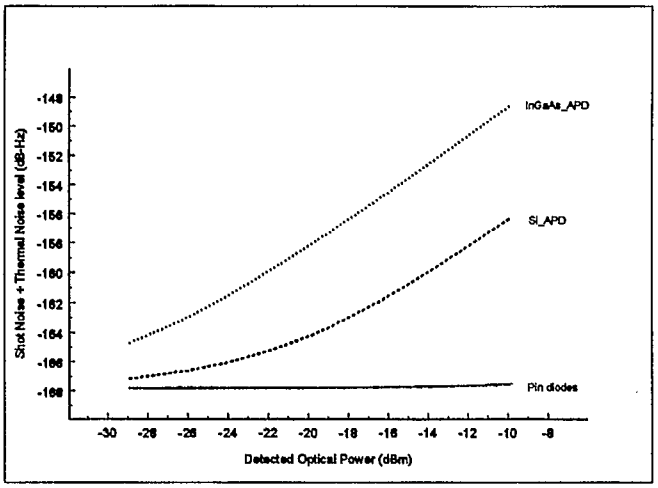

SIGNAL-TO-NOISE RATIO

The signal to noise ratio is then:

$$SNR(i,n,p,r,j,Det,Backsrc) := \frac{S_{rf}(i,n,p,r,Det)}{R_d \cdot \left(N_{s\_sn}(i,n,p,r,Det) + N_{b\_sn}(p,Det,Backsrc) + N_m(Det) + N_{nm}(Det) + N_t\right) \cdot B_{RF_j}}$$

$$SNR_{dB}(i,n,p,r,j,Det,Backsrc) := 10 \cdot \log(SNR(i,n,p,r,j,Det,Backsrc))$$

and in one Hertz

$$SNoR(i,n,p,r,Det,Backsrc) := \frac{S_{rf}(i,n,p,r,Det)}{R_d \cdot \left(N_{s\_sn}(i,n,p,r,Det) + N_{b\_sn}(p,Det,Backsrc) + N_m(Det) + N_{nm}(Det) + N_t\right) \cdot (1 \cdot Hz)}$$

$$SNoR_{dB}(i,n,p,r,Det,Backsrc) := 10 \cdot \log(SNoR(i,n,p,r,Det,Backsrc))$$

Example:

using:

i: Transmit power $P_{L_{i_{tx\_pow}}} = 3 \cdot 10^4 \cdot mW$

r: Range $R_{i_{range}} = 2 \cdot 10^3 \cdot km$

n: Transmit pointing accuracy $\psi_{tx\_pt_{i_{pt}}} = 1 \cdot \mu rad$

p: Antenna diameter $D_{ant_{i_{Dant}}} = 10 \cdot cm$

j: RF bandwidth $B_{RF_{i_{RF}}} = 2.5 \cdot GHz$

we obtain

$$P_{opt\_rx\_dB}\left(i_{tx\_pow}, i_{pt}, i_{Dant}, i_{range}\right) = -14.15 \cdot dBm$$

$$SNR_{dB}\left(i_{tx\_pow}, i_{pt}, i_{Dant}, i_{range}, i_{RF}, InGaAs\_PIN, NO\_BACKGROUND\right) = 30.454 \cdot dB$$

$$SNR_{dB}\left(i_{tx\_pow}, i_{pt}, i_{Dant}, i_{range}, i_{RF}, InGaAs\_APD, NO\_BACKGROUND\right) = 35.515 \cdot dB$$

$$SNR_{dB}\left(i_{tx\_pow}, i_{pt}, i_{Dant}, i_{range}, i_{RF}, Si\_PIN, NO\_BACKGROUND\right) = 28.674 \cdot dB$$

$$SNR_{dB}\left(i_{tx\_pow}, i_{pt}, i_{Dant}, i_{range}, i_{RF}, Si\_APD, NO\_BACKGROUND\right) = 41.051 \cdot dB$$

Detected Optical Signal $Z_{PO\_rx_{i\,pow}} := P_{opt\_rx\_dB}(i_{pow}, i_{pt}, i_{Dant}, i_{range})$

Generated Electrical signal $Z_{Pel_{i\,pow, j\,det}} := S_{rf\_dBm}(i_{pow}, i_{pt}, i_{Dant}, i_{range}, j_{det})$

Total Noise level $N_{total_{i\,pow, j\,det}} := 10 \cdot \log\left[\frac{(N_{s\_sn}(i_{pow}, i_{pt}, i_{Dant}, i_{range}, j_{det}) + N_t) \cdot R_d \cdot Hz}{mW}\right]$

Signal-to-noise ratio

$$ZAB_{i\,pow, j\,det} := S_{rf\_dBm}(i_{pow}, i_{pt}, i_{Dant}, i_{range}, j_{det}) - 10 \cdot \log\left[\frac{(N_{s\_sn}(i_{pow}, i_{pt}, i_{Dant}, i_{range}, j_{det}) + N_t) \cdot R_d \cdot Hz}{mW}\right]$$

Electrical Signal Power generated versus Detected Optical Power

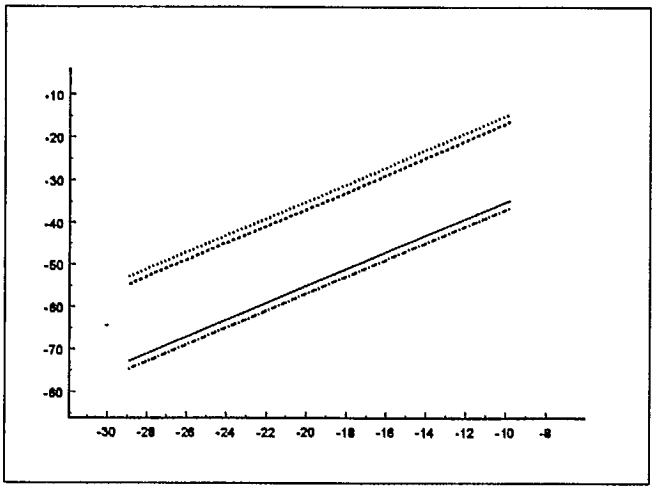

Noise power level versus Detected Optical Power

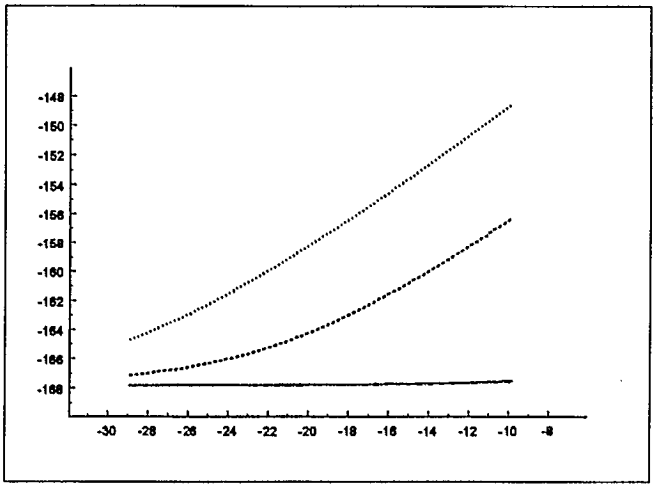

Signal-to-Noise Ratio

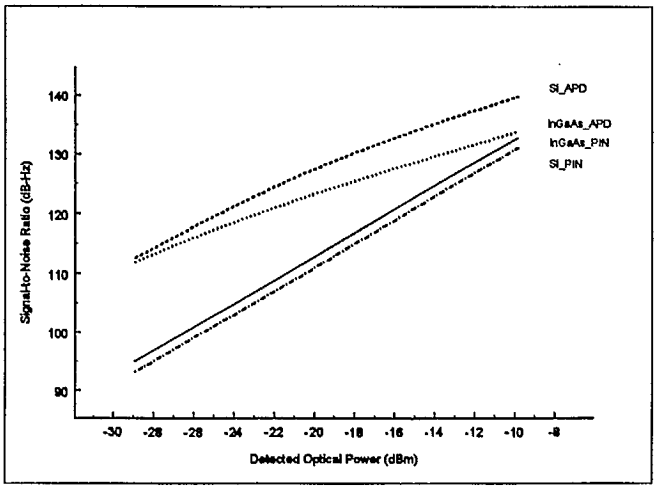

BIT ERROR RATE

Error Function $\quad erf(x) := \frac{2}{\sqrt{\pi}} \cdot \int_0^x e^{-u^2} du \qquad erfc(x) := 1 - erf(x)$

A) Amplitude Shift Keying

The ASK /direct detection optical communication system has a feature that the noise variance is different for a mark and space time slots, because the noise level depends on the input signal (shot noise). This fact makes the calculation of the sensitivity complicated. However, with a few assumption, computation can be made easier. First, assume that the distribution of 1 and 0 is equal (1/2) and that no power is transmitted during a 0. Then defining:

$I_s(i,n,p,r,Detec\_type) := G_{det}(Detec\_type) \cdot \eta_d(Detec\_type) \cdot P_{opt\_rx}(i,n,p,r)$ Signal photocurrent

$I_b(p,Detec\_type,Backsrc) := G_{det}(Detec\_type) \cdot \eta_d(Detec\_type) \cdot P_b(p,Backsrc)$ Background source photocurrent

$$\sigma_1(i,n,p,r,j,Detec\_type,Backsrc) := \sqrt{\left[\begin{array}{l} N_{s\_sn}(i,n,p,r,Detec\_type) \ldots \\ +N_{b\_sn}(p,Detec\_type,Backsrc) \ldots \\ +N_m(Detec\_type) \ldots \\ +N_{nm}(Detec\_type) \ldots \\ +N_t \end{array}\right] \cdot B_{RF_j}}$$

rms photocurrent due to noise during reception of a 1.

$$\sigma_0(p,j,Detec\_type,Backsrc) := \sqrt{\left[\begin{array}{l} N_{b\_sn}(p,Detec\_type,Backsrc) \ldots \\ +N_m(Detec\_type) \ldots \\ +N_{nm}(Detec\_type) \ldots \\ +N_t \end{array}\right] \cdot B_{RF_j}}$$

rms photocurrent due to noise during reception of a 0.

Using the optimal threshold [ref.2p190], the BER fo ASK modulation can be determined by:

$$BER_{ASK}(i,n,p,r,j,Det,Backsrc) := \frac{1}{2} \cdot erfc\left[\frac{I_s(i,n,p,r,Det)}{\sqrt{2} \cdot \left(\sigma_0(p,j,Det,Backsrc) + \sigma_1(i,n,p,r,j,Det,Backsrc)\right)}\right]$$

This optimal threshold is given by:

$$ASK_{th}(i,n,p,r,j,Det,Backsrc) := \frac{\left[\left(I_s(i,n,p,r,Det)\cdot\sigma_0(p,j,Det,Backsrc)\right) + \left(I_b(p,Det,Backsrc)\cdot\sigma_1(i,n,p,r,j,Det,Backsrc\right.\right.}{s_0(p,j,Det,Backsrc) + \sigma_1(i,n,p,r,j,Det,Backsrc)}$$

where:

i = counter on transmit optical power P_L

n = counter on transmit pointing error angle ψ_{tx_pt}

p = counter on antenna diameter D_{ant}

r = counter on range R

j = counter on RF bandwidth B_{RF}

Det = Detector type

Examples

A) Error probability as a function of the power received for various data rates

Assuming:

Wavelength $\lambda = 1.55 \cdot \mu m$

Transmit optical power $P_{L_{40}} = 41 \cdot W$ to $P_{L_{50}} = 51 \cdot W$

Counter on laser power $j_L := 0..imax$

Optical Amplifier gains

Transmit $G_{tx\_opt\_amp\_dB} = 0 \cdot dB$

Receive $G_{rx\_opt\_amp\_dB} = 0 \cdot dB$

Antenna diameter $i_{Dant} := 1$ $D_{ant_{i_{Dant}}} = 10 \cdot cm$

Counter on Antenna diameter $j_{Dant} := 0..pmax$

Pointing error of: $i_{pt} := 0$ $\psi_{tx\_pt_{i_{pt}}} = 1 \cdot \mu rad$

Detector

Counter on Detector type $j_{det} := 0..det\_type\_num$

Range $i_{range} := 8$ $R_{i_{range}} = 4.5 \cdot 10^3 \cdot km$

Counter on range $j_{range} := 0..rmax$

Data rates $B_{RF_0} := 2.5 \cdot GHz$ to $B_{RF_{jmax}} := 7.5 \cdot GHz$

Counter on data rates $j_{BRF} := 0..jmax$

Background Source BACKGND := NO_BACKGROUND

We obtain:

Signal-to-Noise ratio in one Hz $Z0_{j_L, j_{det}} := SNoR_{dB}(j_L, i_{pt}, i_{Dant}, i_{range}, j_{det}, BACKGND)$

Bit error rate

vs data rates for an InGaAs_PIN $Z1_{j_L, j_{BRF}} := BER_{ASK}(j_L, i_{pt}, i_{Dant}, i_{range}, j_{BRF}, InGaAs\_PIN, BACKGND)$

vs detector type for a 2.5 GHz link $Z5_{j_L, j_{det}} := BER_{ASK}(j_L, i_{pt}, i_{Dant}, i_{range}, i_{RF}, j_{det}, BACKGND)$

Received optical power $Z2_{j_L} := P_{opt\_rx\_dB}(j_L, i_{pt}, i_{Dant}, i_{range})$

Link gain $Z3_{j_{range}, j_{Dant}} := P_{opt\_rx\_dB}(0, i_{pt}, j_{Dant}, j_{range}) - 10 \cdot \log\left(\frac{P_{L_0}}{1 \cdot mW}\right)$

Range $Z4_{j_{range}} := \frac{R_{j_{range}}}{1000}$

Link gain versus Distance for various Antenna sizes

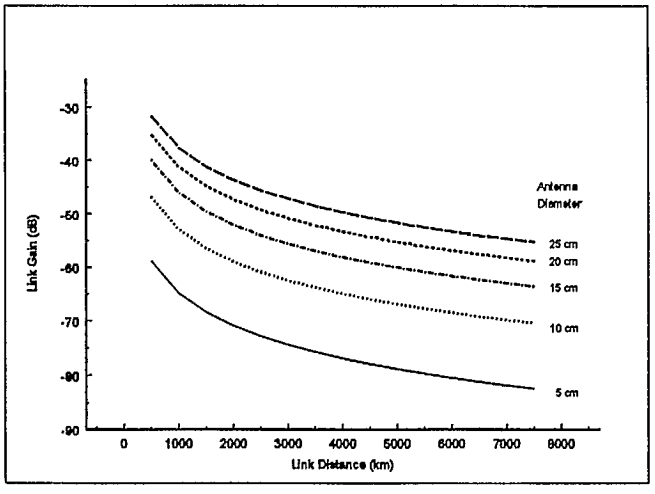

Bit-error rate
versus
Optical received power
for various
Data rates
for an InGaAs_PIN

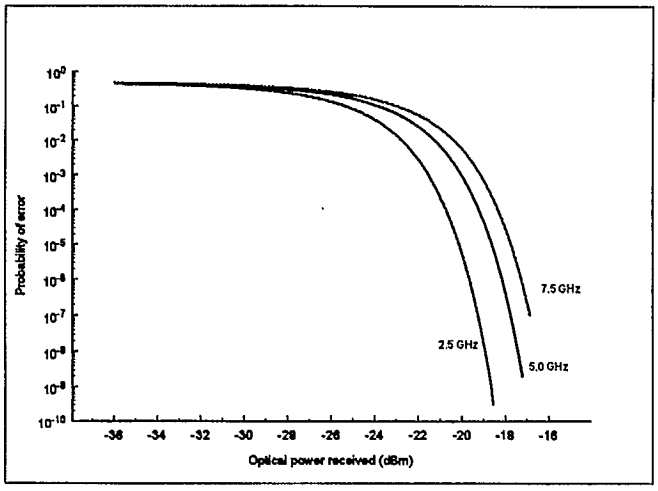

Bit-error rate
versus
Optical received power
for various
photodetectors
for 2.5 Gbps

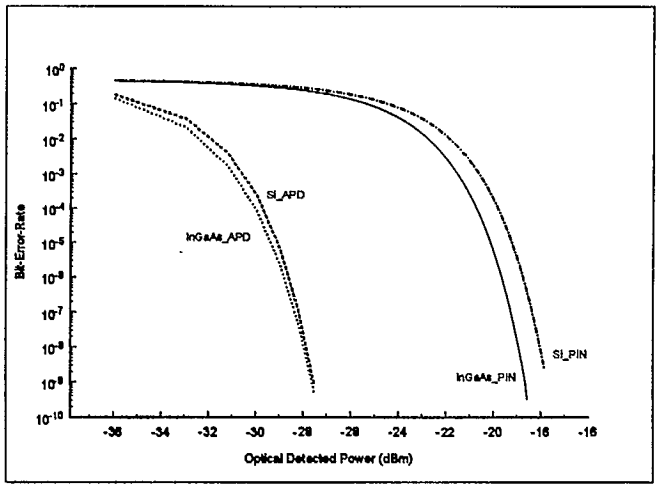

DATE DUE

13. MAY 02			

Communications
Research Centre
Shirleys Bay
3701 Carling Avenue
P.O. Box 11490
Station H
Ottawa, Ontario
K2H 8S2

Centre de recherches
sur les communications
Shirleys Bay
3701, avenue Carling
Case postale 11490
Succursale H
Ottawa (Ontario)
K2H 8S2